nagra.

Technical Report 13-03

Redox properties of iron-bearing clays and MX-80 bentonite – Electrochemical and spectroscopic characterization

March 2014

Th. B. Hofstetter, Y. Sosedova, C. Gorski,
A. Voegelin, M. Sander

eawag, Dübendorf

National Cooperative
for the Disposal of
Radioactive Waste

Hardstrasse 73
CH-5430 Wettingen
Switzerland
Tel. +41 56 437 11 11

www.nagra.ch

nagra.

Technical Report 13-03

Redox properties of iron-bearing clays and MX-80 bentonite – Electrochemical and spectroscopic characterization

March 2014

Th. B. Hofstetter, Y. Sosedova, C. Gorski,
A. Voegelin, M. Sander

eawag, Dübendorf

National Cooperative
for the Disposal of
Radioactive Waste

Hardstrasse 73
CH-5430 Wettingen
Switzerland
Tel. +41 56 437 11 11

www.nagra.ch

This report was prepared on behalf of Nagra. The viewpoints presented and conclusions reached are those of the author(s) and do not necessarily represent those of Nagra.

ISSN 1015-2636

Abstract

The characterization of the redox properties of Fe-bearing minerals in the presence and absence of dissolved Fe^{2+} is of major relevance for the assessment of redox reactions in natural and engineered environments such as radioactive waste repositories. In this study, we developed an electrochemical approach based on the use of soluble organic electron transfer mediators, which enabled us to quantify the redox properties of Fe-bearing clay minerals, MX-80 bentonite and combinations of clay minerals, Fe oxides and dissolved Fe^{2+}. Using mediated electrochemical oxidation and reduction, we quantified the electron accepting and donating capacities of ferruginous smectite SWa-1, Wyoming montmorillonite SWy-2 and MX-80 bentonite at pH 7.5. All structural Fe in clay minerals was redox-active in contrast to that present in other, not further defined phases of MX-80. The materials investigated were redox-active over a very wide range of Eh-values, that is the Fe^{2+}/Fe_{total} ratio of the minerals changed from 0 to 100 % between +600 and -600 mV (vs. SHE). Redox properties were highly path-dependent due to structural changes of the minerals as revealed from the study of native and redox-cycled clay minerals after repeated reduction and re-oxidation cycles. Irreversible alteration of the mineral structure, however, was less obvious for materials with lower total Fe content such as MX-80 bentonite and SWy-2. Systems containing native montmorillonites (SWy-2 or MX-80), goethite and dissolved Fe^{2+} were also able to buffer the reduction potential E_H between 0 and -300 mV. Regardless of their Fe oxidation state, Fe-bearing minerals are redox-active over a wide potential range and therefore very relevant as redox buffers determining the fate of redox-active radionuclides and metals in waste repositories.

Zusammenfassung

Um die Redox-Eigenschaften von natürlichen und bautechnischen Umgebungen wie zum Beispiel die in geologischen Tiefenlagern besser beurteilen zu können, ist die Charakterisierung der Redox-Eigenschaften von Fe-haltigen Mineralen bei An- und Abwesenheit von gelöstem Fe^{2+} von grosser Bedeutung. Im Rahmen dieser Studie wurde ein elektrochemisches Verfahren entwickelt, das lösliche, organische Mediatoren verwendet, um Elektronenübergänge zu messen. Mit diesem Verfahren konnten die Redox-Eigenschaften von Fe-haltigen Tonmineralen, MX-80-Bentonit sowie Kombinationen von Tonmineralen, Eisenoxiden und gelöstem Fe^{2+} quantifiziert werden. Durch elektro-chemisch erwirkte Oxidation und Reduktion von eisenhaltigem Smektit SWa-1, Wyoming-Montmorillonit SWy-2 sowie MX-80-Bentonit konnte deren Fähigkeit zur Elektronenaufnahme und -abgabe bei einem pH-Wert von 7.5 quantifiziert werden. In den Tonmineralen war das strukturell gebundene Eisen redoxaktiv im Gegensatz zum Fe in den nicht weiter definierten Phasen des MX-80-Bentonits. Die untersuchten Materialien waren über ein breites Eh-Spektrum redoxaktiv: das Fe^{2+}/Fe_{gesamt}-Verhältnis der Minerale variierte von 0 bis 100 % zwischen +600 und -600 mV (vs. SHE). Die Redox-Eigenschaften der Minerale waren aufgrund deren struktureller Änderungen, wie sie in nativen oder Redox-belasteten Tonmineralen vorkommen, sehr pfadabhängig. Bei Materialien mit einem niedrigeren Fe-Gehalt, wie in MX-80-Bentonit und SWy-2-Montmorillonit, waren weniger irreversible Veränderungen der Mineralstruktur zu beobachten. Systeme, die aus natürlichen Montmorilloniten (SWy-2 oder MX-80), Goethit und gelöstem Fe^{2+} bestehen, konnten einen Eh-Bereich zwischen 0 und -300 mV puffern. Unabhängig vom Fe-Oxidationszustand sind Fe-haltige Minerale über einen breiten Potenzialbereich redoxaktiv. Aus diesem Grund sind sie als Redox-Puffer, welche das Verhalten von redoxaktiven Radionukliden und Metallen in geologischen Tiefenlagern für radioaktive Abfälle bestimmen, sehr wichtig.

Résumé

Afin de pouvoir évaluer les réactions rédox dans des environnements naturels ou artificiels tels que des dépôts profonds pour déchets radioactifs, il est particulièrement important de caractériser les propriétés rédox des minéraux contenant du fer en fonction de la présence ou de l'absence de Fe^{2+}. Dans le cadre de cette étude, nous avons élaboré une méthode électrochimique faisant intervenir des médiateurs de transfert d'électrons organiques solubles, ce qui nous a permis de mesurer les propriétés rédox de minéraux argileux contenant du fer, de la bentonite MX-80 et de différentes combinaisons de minéraux argileux, d'oxydes de fer et de Fe^{2+} dissous. Par le biais de procédés d'oxydation et de réduction électrochimiques, il a été possible d'étudier le comportement donneur et accepteur d'électrons de la smectite ferrugineuse SWa-1, de la montmorillonite du Wyoming SWy-2 et de la bentonite MX-80 dans un milieu au pH 7.5. On a constaté que l'ensemble du fer structural des minéraux argileux avait une activité rédox, au contraire du fer présent dans d'autres phases de la bentonite MX-80, qui n'ont pas été précisément définies. Les matériaux étudiés avaient une activité rédox couvrant un spectre très large de valeurs E_H, à savoir que le rapport Fe^{2+}/Fe_{total} variait de 0 to 100 % entre +600 and -600 mV (SHE). Les propriétés rédox dépendaient beaucoup des structures transmissives liées aux modifications structurales des minéraux, comme l'a montré la comparaison des minéraux argileux dans leur état original et après des cycles répétés de réduction/réoxydation. Toutefois, on a constaté moins de modifications structurales irréversibles dans les matériaux dont la teneur totale en fer était plus basse, comme dans le cas de la bentonite MX-80 et de la SWy-2. Les systèmes qui contenaient au départ des montmorillonites (SWy-2 ou MX-80), de la goethite et du Fe^{2+} dissous étaient aussi capables de tamponner un potentiel rédox E_H de l'ordre de 0 et -300 mV. Quel que soit l'état d'oxydation du fer, les minéraux contenant du fer ont une activité rédox qui couvre un large spectre. Ils peuvent donc être pris en compte comme tampons rédox ayant une influence sur le comportement des radionucléides et métaux à activité rédox dans les dépôts géologiques pour déchets radioactifs.

Table of Contents

List of Tables

List of Figures

1 Introduction

1.1 Iron-bearing clay minerals as backfill material in waste repositories

According to Nagra's disposal concept for radioactive waste, clays and clay minerals play a decisive role as sealing materials for the attenuation of radionuclide release in the subsurface (Nagra 2002a, 2002b). Bentonite clay is foreseen as buffer material surrounding high-level waste-containing canisters, which are to be emplaced in Opalinus Clay host rock. Canister material options include carbon steel and copper-steel but further options are being investigated. During the evolution of the repository with time, steel canisters can eventually corrode and give rise to an altered matrix in the vicinity of the deposited materials (Kumpulainen et al. 2010). Key components of the altered matrix likely include significant concentrations of dissolved and adsorbed Fe^{2+} as well as various, ferrous iron containing minerals including ferrous oxides, sulfides, carbonates, and iron-bearing clay minerals (Carlson et al. 2006, Milodowski et al. 2009a). Under such reducing conditions, a variety of redox processes can take place that alter both the bulk properties of the bentonite buffer materials as well as those of released radionuclides, that is their redox state and thus their affinity for the sorbent matrix. Reduction of structural Fe increases net negative charge in the mineral structure, the hydration of smectite surfaces, and the cation exchange capacity (CEC). The extent of increase, however, can be compensated by (partial) interlayer collapse, which also leads to a decrease of swelling capacity and specific surface area (Gates et al. 1996, Gates et al. 1993, Gates et al. 1998, Kostka et al. 1999, Stucki et al. 2002, Stucki et al. 2000).

1.2 Processes affecting the radionuclide retention by clay minerals through the presence of ferrous iron in waste repository matrix

The presence of dissolved Fe^{2+} in µM concentrations from the corrosion of steel canisters can, in principle, induce a variety of geochemical processes at clay mineral surfaces that might directly or indirectly affect its sorbent properties of the sealing material. First, ferrous iron is a competitor of cationic radionuclides for the cation exchange capacity of the clay leading to a decreased retention of radionuclides. Second, reaction of Fe^{2+} with clays can alter the sealing materials in different ways. Current hypotheses include the neoformation of iron-rich smectites, (Carlson et al. 2006) in which iron constitutes a part of the mineral structure or – assuming that the clay buffers already contain some iron in the crystal lattice – reduction of structural Fe^{3+}. The latter is frequently observed as interfacial electron transfer reaction between sorbed Fe^{2+} and structural Fe^{3+} in iron oxides (Cwiertny et al. 2008, Gorski & Scherer 2011, Larese-Casanova & Scherer 2007, Mikutta et al. 2009, Williams & Scherer 2004, Yanina & Rosso 2008) but has not yet been investigated systematically with iron-containing clay minerals.

Recent work with smectite clay minerals implies that at least partial interfacial electron transfer from adsorbed to structural iron is possible (Schaefer et al. 2011, Soltermann et al. 2013). As shown for many other reductants and microbes, a change of Fe redox state is often accompanied by changes of relevant mineral parameters (Drits & Manceau 2000, Komadel et al. 1990, Komadel et al. 2005, Komadel et al. 1995, Komadel et al. 2006, Kostka et al. 1999, Manceau et al. 2000a, Manceau et al. 2000b, Stucki et al. 1996, Stucki et al. 2002, Yan & Stucki 2000). Such alterations can affect crucial endpoints for radionuclide retention via adsorption such as the cation exchange capacity and the surface area of oxidized vs. reduced smectites. In addition, structural Fe^{2+} in smectites can also act as reductant as was shown for organic compounds (Hofstetter et al. 2006, Hofstetter et al. 2003, Neumann et al. 2008, Neumann et al. 2009, Neumann et al. 2011a) and some redox-active metals and radionuclides (Bradbury & Baeyens

2005b, Ilton et al. 2006, Soltermann et al. 2013). Because changes in oxidation state of the latter also alter their charge and thus the adsorption behavior, knowledge of iron redox processes of clay minerals is crucial for assessing the long-term integrity of waste repositories.

1.3 Scientific challenges of understanding processes underlying redox-active behavior of clay minerals

Systematic evaluations of radionuclide adsorption to clay minerals have been carried out with minerals in their oxidized state (Bradbury & Baeyens 2005a, Bradbury & Baeyens 2005b, Bradbury & Baeyens 2009a, Bradbury & Baeyens 2009b) but are lacking for iron-containing clay minerals under reducing conditions. The main reasons for this research gap is the limited understanding of structural Fe equilibrium redox chemistry and the lack of experimental approaches that allow for controlling the Fe redox state in clays minerals. New approaches are currently pursued to quantify the intrinsic redox properties, that are the reduction potentials, E_H, of the redox pair Fe^{2+}/Fe^{3+} in the clay mineral lattice. Furthermore, additional knowledge is required to assess if and how E_H-values depend on mineral properties such as total Fe content, degree of Fe reduction, and its structural arrangements and how they can be detected with spectroscopic tools.

1.3.1 Arrangement of structural Fe in clay minerals

In fact, various spectroscopic studies including infrared, UV-visible, X-ray absorption, and Mössbauer spectroscopy of chemically and biologically reduced and re-oxidized Fe-bearing clay minerals have elucidated the processes affecting the coordination and redox state of Fe within the octahedral sheet (Neumann et al. 2011a, Neumann et al. 2011b). Chemical reduction of structural iron is usually carried out with dithionite, which results in a "pseudo random" distribution of Fe^{2+} within the octahedral sheet (Lear & Stucki 1987). Fe^{2+} generated in the mineral structure by partial reduction is preferentially located near Fe^{3+} ions. As confirmed by investigation of absorption bands for Fe^{2+}-O-Fe^{3+} inter-valence electron transfer, Fe^{2+}-Fe^{3+} pairs form in a way that Fe ions must occupy adjacent octahedral sites (Hunter & Bertsch 1994, Hunter et al. 1999, Komadel et al. 2006). Fe^{2+}-Fe^{2+} entities, in contrast, were postulated to be generated only after reduction of all Fe^{3+}-Fe^{3+} to Fe^{2+}-Fe^{3+}, which corresponds to Fe^{2+}/Fe_{total} of approximately 50 % (Lear & Stucki 1987). The same trends of absorption bands of Fe^{2+}-O-Fe^{3+} inter-valence electron transfer were observed upon re-oxidation of structural Fe^{2+}, which implied sequential oxidation of Fe^{2+}-Fe^{2+} to Fe^{2+}-Fe^{3+}, followed by complete oxidation to Fe^{3+}-Fe^{3+} groups. This pattern of Fe reduction and re-oxidation was taken to support electron transfer via the basal siloxane planes of the clay minerals because an electron transfer from the edge surfaces would result in larger, distinct domains of Fe^{2+} and Fe^{3+} (Komadel et al. 1990, Komadel et al. 2006).

For dioctahedral smectites, reduction mechanisms of Fe^{3+} to Fe^{2+} have been proposed that account for structural alterations and changes in clay properties such as increasing surface charge (Drits & Manceau 2000, Lear & Stucki 1989). With increasing degree of reduction, Fe^{2+} ions migrate from cis-octahedra to adjacent trans-octahedra yielding trioctahedral Fe^{2+} clusters, which are separated by domains of vacancies. A schematic of these processes is given in Fig. 1 for structural changes in the octahedral sheet of ferruginous smectite (SWa-1; Neumann et al. 2008). Reduction is accompanied by a dehydroxylation reaction owing to the protonation of OH groups initially coordinated to Fe^{3+} (Manceau et al. 2000a, Manceau et al. 2000b). The negative excess charge after Fe^{3+} reduction is localized at the O-ligands at the boundary between trioctahedral and vacancy domains and is compensated by the uptake of protons and cations from solution (Drits & Manceau 2000, Manceau et al. 2000a). This mechanism of Fe^{3+} reduction was

proposed only for trans-vacant smectites while cis-vacant smectites did not tend to form trioctahedral domains due to higher activation energy for the involved structural rearrangements (Drits & Manceau 2000).

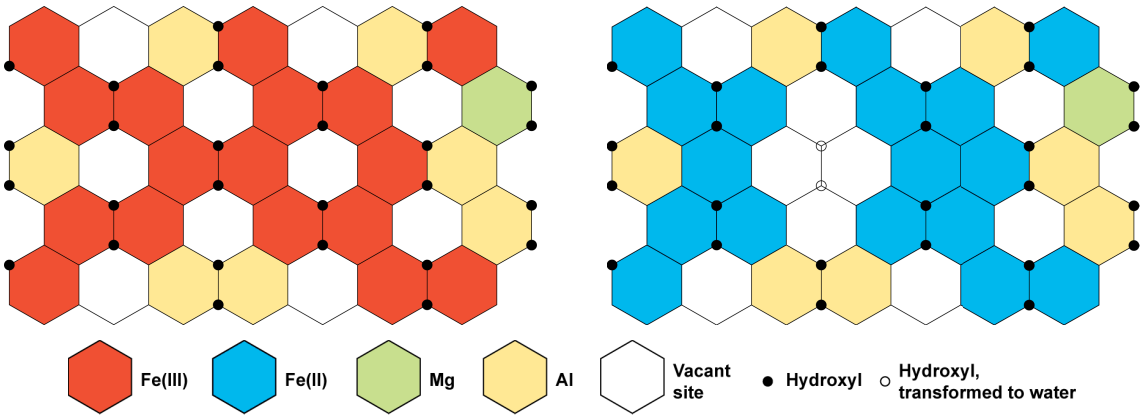

Fig. 1: Schematic representation of octahedral cationic arrangement derived from IR spectroscopy in the structure of (a) unaltered and (b) completely reduced trans-vacant ferruginous smectite.

During reduction, structural rearrangements lead to the formation of trioctahedral Fe^{2+} groups enclosing domains of vacancies and to the dehydroxylation of the octahedral sheet (indicated as open circle in (b)). Only those cations sharing a hydroxyl group (black filled circle) can be investigated in the middle and near infrared regions (Neumann et al. 2011a, Neumann et al. 2011b).

The degree of reversibility of structural modifications observed during structural Fe^{3+} reduction in clay is still controversial. Reversibility was hypothesized to depend on various concurrent factors such as the nature of the reductant or oxidant, the total Fe content, and the degree of Fe reduction. Similar structural changes were observed for clays reduced to comparable extents by microbes and by dithionite, and, in both cases, the original structure was restored after re-oxidation with molecular oxygen. However, other studies suggest that reduction by microbes resulted in partial reductive dissolution (Kostka et al. 1999) or illitization of smectites (Kim et al. 2004). Irreversible structural modifications are more likely upon reduction of iron-rich clays (Fialips et al. 2002a, Fialips et al. 2002b). These findings were substantiated by a comparative analysis of the reversibility of structural changes in four smectites, monitored via characteristic IR bands from metal-OH bending and Si-O stretching vibrations (Neumann et al. 2008). Even high degrees of Fe^{3+} reduction (75 wt.-% Fe_{tot}) in montmorillonite (3 wt.-% Fe_{tot}) did not cause irreversible structural alterations, while the original structure of ferruginous smectite (13 wt.-% Fe_{tot}) or synthetic nontronite (33 wt.-% Fe_{tot}) could not be fully restored upon re-oxidation of the reduced forms with oxygen or nitroaromatic compounds. Irreversibility of structural changes during a reduction/re-oxidation cycle was observed primarily if the degree of reduction exceeded 50 % of the total Fe content.

The identification of different structural entities of Fe in clay minerals and their dynamic re-arrangement illustrates that quantifying Fe redox properties is not trivial. Several types of Fe species can exist simultaneously within the mineral structure and will exhibit different reduction potentials. Because the extent and the kinetics of electron transfer to and from Fe are determined by the thermodynamic properties of Fe, their quantification is key to understand the mineral redox properties.

1.3.2 Assessing redox properties of Fe in clay minerals

From the reasons illustrated above, it becomes apparent that new approaches are needed to quantify the intrinsic redox properties of structural Fe in clay minerals. This task requires one to determine the key thermodynamic parameter that describes the reactivity of Fe, the reduction potentials, E_H, of various Fe^{2+}/Fe^{3+} arrangements in the clay mineral structure. E_H can best be determined electrochemically, which allows deriving E_H-values as a function of mineral variables, including its structure, iron content, Fe^{2+}/Fe^{3+} ratio, and of solution conditions (e.g., pH). Moreover, electrochemical techniques also enable accurate control of the E_H and quantification of electron accepting and donating capacities of Fe in clay by continuous monitoring of reducing and oxidizing currents, respectively. Electrochemical techniques have previously been used with success to characterize similar systems of Fe oxides exposed to aqueous Fe^{2+} (Grygar 1997, Grygar et al. 2002, Silvester et al. 2005) but no such data is available to date for clay minerals.

The electrochemical characterization of clay minerals, however, is nontrivial. Direct measurement of the reduction potential E_H of Fe in clay suspensions in water is difficult if not impossible, as it requires that particles reach equilibrium with the electrode and solution (Bard & Faulkner 2001a, Silvester et al. 2005) To avert this issue, electrodes have been modified in two ways: (1) using a method where powder is directly packed into a junction between the electrode and solution, known as a powder disk electrode (PDE) (Grygar 1997, Grygar et al. 2002, Nurmi et al. 2004, Nurmi & Tratnyek 2008); or (2) direct deposit of the clay onto the electrode surface (Charradi et al. 2009, Therias et al. 1996, Xiang & Villemure 1995). These methods have been used with some success to measure the potential of iron oxides (Grygar 1997, Grygar et al. 2002, Silvester et al. 2005), but are less explored for iron-bearing clays (Aeschbacher et al. 2010). All the methods mentioned require that the mineral is a good conductor, and is capable of reaching redox equilibrium with the electrode and solution; if the clay is poorly conductive, however, it may be impossible to characterize it using these method. To overcome such issues, we used mediated electrochemical reduction (MER) and oxidation (MEO) in this study. This method has successfully been applied to the redox characterization of a diverse set of humic substances, the major constituent of natural organic matter (Aeschbacher et al. 2012a, Aeschbacher et al. 2012b, Aeschbacher et al. 2010, Aeschbacher et al. 2011, Page et al. 2012).

MER and MEO is achieved by organic radicals that facilitate the electron transfer and hence the attainment of redox equilibrium between the working electrode and the organic or mineral phase studied. As such, this approach has several advantages over previously used, indirect methods that relied on the use of chemical bulk reductants and oxidants. The advantages included (a) a direct quantification of the electrons transferred to and from Fe in clay minerals by integration of reductive and oxidative current responses over time (i.e. chronocoulometry), respectively and (b) control of reduction and oxidation potentials via the potentiostat and pH via an automated titration unit, which allows for quantifying the proton to electron stoichiometry during reductions and oxidations.

1.4 Objectives and approach of the present study

Based on the above considerations, the present study aims contributing to the assessment of redox properties of iron-bearing clay minerals as backfill material in radioactive waste repositories. The specific *study objectives* were:

1. to establish an electrochemical method for the characterization of redox properties pertinent to Fe-bearing clay minerals using well-defined reference materials
2. to determine the electron donating and accepting capacities of the bentonite standard MX-80 and its apparent reduction potential, $E_H^{\emptyset}$, at an ambient pH value of 7.5, as well as
3. to characterize the redox properties of a mixed-phase model system containing redox-active phases that are anticipated to be present in radioactive waste repositories, that is Fe-bearing clay minerals, Fe oxides, and dissolved Fe^{2+}

1.4.1 Using electrochemical approaches for clay minerals

This study is the first to apply mediated electrochemistry for the characterization of iron-bearing clay minerals. The investigation of potential backfill material such as MX-80 bentonite therefore required a preceding evaluation of the proposed method with reference materials as stated in *Study Objective No. 1*. To this end, procedures for mediated electrochemical reduction and oxidation were developed using two source clay minerals of different total Fe content, that is, ferruginous smectite (SWa-1) and Wyoming montmorillonite (SWy-2). Some properties of the solid phases used are summarized in Tab. 1.

Tab. 1: Overview of clay minerals and solids used in this project and their selected properties.

Objective	**Mineral**		**Fe-content**	**Redox treatment**
		[wt.-%]	[$mmol_{FE}/g_{clay}$]	
1. Method development	SWa-1	12.6 ± 0.1	2.26 ± 0.02	Native Reduced Re-oxidized Re-reduced Re-re-oxidized
	SWy-2	2.3 ± 0.2	0.41 ± 0.04	Native Reduced Re-oxidized Re-reduced
2. Backfill material characterization	MX-80	2.4 ± 0.2	0.43 ± 0.04	Native Reduced Re-oxidized

Another challenge in characterizing clay mineral redox properties is that the reduction and oxidation of structural Fe is complex. Structural alterations in the mineral occur as a result of changing the mineral charge balance and the different sizes of Fe^{2+} and Fe^{3+} atoms and may be partially or completely irreversible (Anastacio et al. 2008, Bzdek & McGuire 2009, Dong et al. 2009, Fialips et al. 2002a, Fialips et al. 2002b, Komadel et al. 1995, Kostka et al. 1999, Manceau et al. 2000a, Neumann et al. 2011a, Ribeiro et al. 2009, Rozenson & Heller-Kallai

1976, Russell et al. 1979). To account for how the redox properties of structural Fe are linked to its local coordination environment, a comparison of the electron transfer to and from Fe in clay minerals in "oxidized" (≈ 100 % Fe^{3+}) and "reduced" state (≈ 100 % Fe^{2+}) is needed. Here we use three distinctly prepared minerals with different redox histories to elucidate potentially irreversible structural changes: (a) the purified mineral it its native, that is oxidized state (henceforth re-ferred to as"native" mineral), (b) samples reduced chemically with dithionite ("reduced"), (c) "re-oxidized" and "re-re-oxidized" minerals that were subject to one or two dithionite reduction steps and subsequent oxidation(s) with H_2O_2; (d) "re-reduced" samples correspond to dithionite reduced "re-oxidized" specimen. To relate the measured redox properties to changes in the structural Fe coordination environment, we carried out X-ray absorption (XAS) and ^{57}Fe Mössbauer spectroscopy.

Study Objective No. 2 was carried out with MX-80 bentonite based on the experimental procedures derived for reference materials SWa-1 and SWy-2, respectively. No additional spectroscopic characterization was made.

1.4.2 Evaluation of mixed-phase systems

The apparent reduction potentials of mixed-phase model system were tested with different redox-active minerals in the presence of dissolved Fe^{2+} in study objective no. 3. To obtain first insights into the factors controlling the reduction potential of mixed-phase systems as they exist in contaminated environments, we quantified the effect of Fe^{2+}concentrations on the E_H in suspensions containing either Fe^{2+} associated with an Fe oxide (goethite), SWy-1 as model for a iron-bearing clay mineral, and MX-80 bentonite. The combination of the two solid phases in presence of Fe^{2+} enabled the identification of the phase controlling either the reductant concentration (i.e., Fe^{2+}) and the system's E_H-value. An exploratory mixed phase experiment with MX-80 instead of SWy-2 was also carried out. A list of model systems and experimental conditions is given in Tab. 2.

Tab. 2: Mixed-phase model systems for repository-like conditions explored in this study.

Minerals	**Solid load** [g L^{-1}]	**Fe^{2+}_{total}** [mM]	**pH**
Single phase experiments			
Goethite	0.2 – 2.0	0.15 – 3.6	6.75 – 7.75
SWy-2	0.01 – 0.5	0.3 – 4.7	7.25 – 7.75
MX-80	0.01 – 0.5	0.3 – 3.3	7.5
Mixed phase experiments			
Goethite/SWy-2	0.5/0.015 – 0.5 * 0.1 – 1.0/0.1 **	1.0 1.0	7.5 7.5
Goethite/MX-80	0.1 – 2.0/0.1 **	1.0	7.5

* constant goethite/variable clay mineral concentration
** variable goethite/constant clay mineral concentration

2 Experimental Investigations

2.1 Chemicals

Commercially available chemicals were of analytical grade or higher purity and used without further treatment (Tab. 3). Three electron transfer mediators, that is, triquat (1, 1'-trimethylene-2, 2'-bipyridyl dibromide, TQ), cyanomethyl viologen (1, 1'-bis(cyanomethyl)-4, 4'-bipyridyl, CMV), and a zwitterionic viologen (N,N'-bis(sulfonatopropyl)-4,4'-bipyridyl, ZwiV) were synthesized following procedures described by Gorski et al. (2012b, c, 2013). All aqueous solutions were prepared using nanopure water (resistivity > 18 MΩ·cm, Nanopure Diamond Water System).

2.2 Minerals, clay minerals preparation and their chemical modification

Ferruginous smectite (SWa-1), Wyoming montmorillonite (SWy-2) were purchased from the Source Clay Mineral Repository (Purdue University, West Lafayette, IN). A sodium bentonite MX-80 was obtained from Nagra. Goethite was kindly provided by the lab of Michelle M. Scherer (University of Iowa).

Clay minerals were purified, Na+-saturated, and size fractionated according to the method of Baeyens & Bradbury (1997) as described by Gorski et al. (2012b). Clay minerals were broken up by milling and added to 1 M $NaClO_4$. The suspensions were stirred for three hours, then allowed to settle. The supernatant was discarded and the bottle was re-filled with fresh 1 M $NaClO_4$. This process was repeated three times. Aliquots of the clay mineral suspension were centrifuged at 600 g for seven minutes, with the ≤ 0.5 μm size fraction remaining in the supernatant. The supernatant was decanted and saved, and the centrifuge bottle was refilled with DI water, shaken, and re-centrifuged. This process was repeated until the supernatant remained clear after centrifugation. The fine clay fraction (i.e., the decanted suspension from centrifugation) was then flocculated by the addition of 1 M $NaClO_4$. This suspension sat undisturbed overnight, then the supernatant was removed and discarded. To remove any loosely-bound Fe and Fe (oxyhdr)oxide impurities, a portion of this clay suspension was acidified with HNO_3 to pH 3.5 and stirred for one hour, with the pH monitored and re-adjusted as needed. The suspension was then centrifuged and re-suspended in 1 M $NaClO_4$ at neutral pH. The final clay mineral concentration was typically in the range of 5 – 10 g L^{-1}.

Dithionite-reduced clay minerals were generated inside the glovebox following standard procedures (Hofstetter et al. 2003, Stucki et al. 1984). An aliquot of the clay mineral stock suspension was brought into the glovebox after purging with Ar. 1 M $NaHCO_3$ and 0.3 M Na_3-citrate were then added to the clay mineral suspension. This suspension was then mixed and heated to 70 °C, at which point sodium dithionite was added (3 × the clay mineral mass in suspension) and the suspension was stirred at 70 °C overnight. A portion of the suspension was then taken and put into a pre-washed and dried dialysis tube (MWCO 12400 Da, Sigma Aldrich), and added to 1 L of de-oxygenated 0.1 M $NaClO_4$. The suspension equilibrated for at least eight hours, at which point the dialysis tubing was placed into fresh $NaClO_4$ buffer. This process was repeated four times. Native clay mineral samples were produced in an identical manner, except that no sodium dithionite was added to the citrate-bicarbonate buffer.

Tab. 3: Suppliers, commercially available chemicals used in this study and purities.

Chemical	**Trivial name** (abbreviation)	**Purity** [%]
Sigma-Aldrich		
1, 1'-Diethyl-4, 4'-bipyridyl dibromide	Ethyl viologen (EtV)	99.5
1, 1'-Ethylene-2, 2'-bipyridyl	Diquat (DQ)	100
1,10-Phenantroline		99
2, 2'-Azino bis(3-ethyl benzothiazoline 6-sulfonic acid) diammonium	(ABTS)	99
7-Hydroxy-3H-phenoxazin-3-one sodium salt	Resorufin sodium salt	
3-Morpholino propane sulfonic acid	(MOPS)	99.5
Ammonium acetate		99
Hexaammineruthenium(II) chloride		≥ 99.9
1,4-Naphtoquinone		97
Potassium ferricyanide		99
Riboflavin-5'-phosphate sodium salt hydrate	Flavin mononucleotide (FMN)	73 – 79
Fluka		
Citric acid monohydrate		99.5
2,6-Dichlorophenolindophenol sodium salt hydrate		≥ 90
Ferrous ethylenediammonium sulfate tetrahydrate		≥ 99
Sodium bicarbonate		99.5
Sodium dithionite		80
Sodium hydroxide		32
Sodium perchlorate monohydrate		99
Hydrochloric acid		32
Merck		
Hydrogen peroxide		30
Sodium chloride		99.5
Sulfuric acid		95 – 98
Synchem OHG		
1, 1'-Trimethylene 2, 2'-bipyridyl (triquat)		99
Arcos		
Methanol		99.9

Re-oxidized and re-re-oxidized clay minerals were oxidized by putting an aliquot of the reduced or re-reduced mineral suspension into dialysis tubing which was placed inside 1 L of 0.1 M $NaClO_4$ outside of the glovebox. H_2O_2 (30 %) was then added to the solution in approximately 2:1 stoichiometric excess to the structural Fe in the SWa-1 sample, and the suspension sat overnight in the dark. The dialysis tubing was then transferred three times into fresh 0.1 M $NaClO_4$ solution (1 L) outside the glovebox, and allowed to equilibrate at least eight hours between exchanges. The re-oxidized and re-re-oxidized clay mineral suspensions were then removed from the dialysis tubing and was purged with 99.999 % Ar gas for at least two hours

prior to transferring the suspension back into the glovebox. Re-reduced suspensions were prepared with dithionite as indicated above from re-oxidized clay mineral samples. A survey of clay mineral specimen treated in different redox cycles in shown in Tab. 1.

Clay mineral concentrations were determined gravimetrically by drying the suspension at 105 °C while accounting for the $NaClO_4$-content. The Fe content of the clay minerals was measured according to an established acidic digestion method (Neumann et al. 2008, Neumann et al. 2011a) adapted from earlier references (Amonette & Templeton 1998, Stucki 1981), using ferrous ethylenediammonium sulfate tetrahydrate as the Fe standard. Fe was measured as dissolved Fe^{2+} using the 1,10-phenanthroline method (Harvey et al. 1955). Fe^{2+}-containing suspensions were filtered through a 0.45 µm syringe filter (13 mm PTFE with GMF, BGB Analytik, USA) prior to analysis.

2.3 Anaerobic experiments

All experiments were conducted in an anaerobic glovebox (< 0.1 ppm O_2) with an N_2 atmosphere (M. Braun Inertgas-Systeme GmbH). Plastic and glassware were evacuated over-night in the exchange chamber and allowed to equilibrate in the glovebox atmosphere for several days prior to use. All aqueous solutions and methanol were purged with 99.999 % Ar gas for 2 h prior to transferring them into the glovebox.

2.4 Electrochemistry

Electrochemical experiments were controlled with a 630D electrochemical analyser (CH Instruments, Austin, TX, USA) as outlined in detail in Gorski et al. (2012b). Potentials were measured versus an Ag/AgCl reference electrode and are reported here versus the standard hydrogen electrode (SHE). MER and MEO experiments were carried out in electrochemical cells containing buffer, a cylindrical vitreous carbon working electrode (WE), a Pt wire counter electrode separated from the WE compartment by a glass frit, and an Ag/AgCl reference electrode.

Electron transfer mediators were used to facilitate electron transfer between the working electrode (WE) and Fe of clay minerals and goethite. Mediators were selected for this study based on a series of criteria, namely; each mediator (i) reached apparent redox equilibrium with the working electrode and the mineral, (ii) was stable over the course of the experiment (≈ 6 hrs), (iii) was sufficiently water soluble, and (iv) had a well-defined standard reduction potential (E_H^0) and a known reaction stoichiometry. Owing to issues of mediator adsorption to some of the materials used, two distinct sets of ET-mediators were used as listed in Tab. 4. Two sets of mediators were selected to cover the E_H^0-stability range of water, with E_H^0-values ranging from -0.54 V to +0.70 V (Tab. 4). The first mediator set of one-electron transfer mediators was used in experiments with SWa-1 and goethite suspensions, while the second set containing zwitterionic and anionic mediators was used with SWy-2 and MX-80. Each mediator was used at E_H-values within ± 0.12 V of its E_H^0-value (Fultz & Durst 1982, Meckstroth et al. 1981).

Cyclic voltammetry (CV) experiments were conducted to verify the E_0 of the mediators. To this end, a 8 – 10 mL solution of buffer containing a 3.0 mm diameter glassy carbon disk working electrode, a platinum wire counter electrode, and an Ag/AgCl reference electrode. CV scans were done at 10 mV sec^{-1} over a potential range of approximately ± 0.3 V of the expected $E_H^{0'}$ values.

Tab. 4: Electron transfer mediator sets used in this study

Abbreviation	Chemical	E_H^0 [V]
Set 1: One-electron transfer mediators		
TQ	Triquat (1, 1'-trimethylene-2, 2'-bipyridyl)	-0.54
EtV	Ethyl viologen (1, 1'-diethyl -(4, 4'-bipyridyl))	-0.45
ZwiV	Zwitterionic viologen (N,N'-bis(sulfonatopropyl)-4,4'-bipyridyl)	-0.38
DQ	Diquat (1, 1'-ethylene-2, 2'-bipyridyl)	-0.35
FMN	Flavin mononucleotide (riboflavin-5'-phosphate)	-0.22
CMV	Cyanomethyl viologen (1, 1'-bis(cyanomethyl)-4, 4'-bipyridyl)	-0.14
Ru	Hexaammineruthenium ($Ru^{2+/3+}(NH_3)_6$)	+0.09
FeCN	Ferri/ferro-cyanide ($Fe^{2+/3+}(CN)_6$)	+0.43
ABTS	2, 2'-Azino bis(3-ethyl benzothiazoline 6-sulfonic acid)	+0.70
Set 2: Two-electron transfer mediators		
RSR	Resorufin	-0.06
NQ	1,4-Naphtoquinone	+0.06
DCPIP	2,6-Dichlorophenolindophenol	+0.22

In MER and MEO experiments (Fig. 3), an electrochemical cell containing 80 mL of pH buffer was pre-equilibrated at the applied E_H until the current (I) plateaued. A known amount of mediator (10 µmol) was then added to the cell. After the current returned to the baseline value, indicating that the mediator redox couple and WE were in redox equilibrium, small aliquots (10 - 100 µL) of clay mineral stock suspensions were spiked into the electrochemical cell (at least 4 spikes per experiment). Integration of the current peaks yielded the number of electrons transferred between structural Fe in the clay mineral and the WE (eq. 1):

$$q = \frac{1}{F} \cdot \int_{1_1}^{1_2} I \cdot dt \quad (1)$$

where q is the number of electrons transferred in moles, F is the Faraday constant (96'485 C/mol), and t is time. Peak integration was done using Igor Pro software (Wavemetrics, Lake Oswego, OR, USA).

To quantify the *electron accepting capacities* (Q_{EAC}, $mol_e\text{-}/g_{clay\ mineral}$) of the clay minerals, MER was performed by spiking TQ^{2+} into the electrochemical cell (10 µmol) after the WE was pre-equilibrated at E_H = -0.60 V. Likewise, the *electron donating capacity* (Q_{EDC}, $mol_e\text{-}/g_{clay\ mineral}$) was measured by MEO with an experiment setup similar to MER, except that ABTS was oxidized to $ABTS^{\bullet+}$ at the WE, which was polarized to E_H = +0.61 V. Electron donating and accepting capacities were obtained by normalizing the amount of electrons transferred with the clay mineral mass as in eq. 2. For SWy-2 and MX-80, Q_{EAC} was determined at E_H of -0.55 V and Q_{EDC} at E_H = +0.64 V using ZwiV and ABTS as ET-mediators, respectively.

$$Q_{EAC,EDC} = \frac{q}{m} \quad (2)$$

where q is the number of electrons transferred in moles as in eq. 1 and m is the clay mineral mass in g.

2.5 Spectroscopy

2.5.1 X-ray absorption spectroscopy (XAS)

Clay mineral suspensions were dried in the glovebox (reduced samples) or in air (native and oxidized samples), mixed with cellulose and boron carbide, and pressed into pellets (oxic: 10 mm diameter, reduced: 7 mm diameter). Fe K-edge X-ray absorption near edge structure (XANES) and extended X-ray absorption fine structure (EXAFS) spectra were measured at the XAS beamline at the Angströmquelle Karlsruhe (ANKA, Karlsruhe, Germany). The spectra were recorded in transmission mode using a Si(111) double crystal monochromator (DCM) in a closed cycle He cryostat cooled to 15 K. The monochromator energy was calibrated by setting the first inflection point of the absorption edge of a Fe metal foil to 7111 eV (Wilke et al. 2001). The spectra were processed and analysed using Athena and Artemis software (Ravel & Newville 2005).

2.5.2 ^{57}Fe Mössbauer spectroscopy

Samples for Mössbauer analysis were filtered, dried, and ground in the anaerobic glovebox prior to analysis. Measurements were made using a previously described setup (Larese-Casanova & Scherer 2007). Spectra were fit using the commercial software Recoil (Ottawa, Canada) and a Voigt-based model (see fit parameters in Gorski et al. 2012b, Rancourt & Ping 1991). ^{57}Fe Mössbauer spectra were collected for each smectite at 13 K after the purification procedure to determine the structural coordination and oxidation state of the Fe. Spectra collected at 40 K were consistent with 13 K spectra. All spectra were characteristic of Fe^{3+} in clay minerals, with no indication of any Fe^{2+} phases or Fe^{3+} (oxyhydr-)oxide impurities (detection limit ≈ 1 - 2 % Fe) (Dyar et al. 2008). The fitted hyperfine parameters of SWa-1 and SWy-2 indicated that the minerals contained only *cis*-octahedral Fe^{3+} ($^{Oct}Fe^{3+}$; i.e., the two binding hydroxyl groups were adjacent to one another).

2.6 Experimental approaches for the investigation of mixed-phase systems

2.6.1 Sorption of electron transfer mediators and mediator selection for E_H-measurements

Sorption isotherms of one- and two-electron transfer mediators were quantified for goethite and SWy-2 in batch experiments under oxic conditions. To this end, reactors contained variable concentrations of mediators (up to 175 µM) in 0.1 M $NaClO_4$ and 0.1 M MOPS at pH 7.5, and were equilibrated with either 1 g L^{-1} of goethite or 0.1 g L^{-1} SWy-2 under continuous stirring. Dissolved mediator concentrations were measured by UV/Vis photometry in PMMA or 1 cm quartz cuvettes at selected wavelengths for different mediators (i.e., 295 nm for DQ, 284 nm for EtV, 286 nm for ZwiV, 286 nm for CMV, 295 nm for TQ). Suspensions were centrifuged at 10^4 rpm at room temperature for 5 min and the supernatant was transferred into cuvettes for subsequent UV/Vis measurement. The amount of mediator sorbed was calculated from the difference between the initial in absence of solid and the final measurement in suspension. Results were normalized to the clay mass. A compilation of sorption isotherms is shown in Fig. 2.

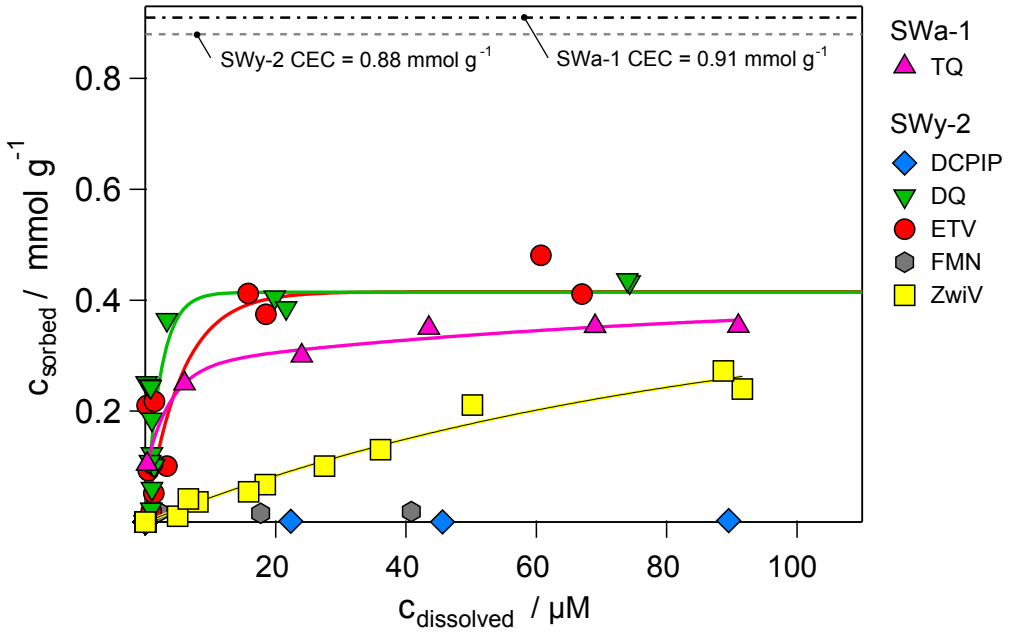

Fig. 2: Sorption isotherms of oxidized DCPIP, DQ, EtV, FMN and ZwiV mediators on native SWy-2 (full markers) and of oxidized TQ on native SWa-1 (empty markers) at pH = 7.5.

Owing to its high surface charge density, electron acceptors and cations such as TQ generally adsorb only moderately to SWa-1 in agreement with previous work with nitroaromatic compounds (Hofstetter et al. 2006). As illustrated for the TQ adsorption to SWa-1, the measured current response for an addition of approximately clay mineral spikes was approximately an order of magnitude larger than the expected current response if the cationic form (TQ^{2+}) preferentially sorbed. For SWy-2, however, sorption of cation mediator species was substantial and compromised MEO/MER experiments (data not shown). We therefore used the ZwiV as mediator.

2.6.2 Reduction potential measurements in the presence of dissolved Fe^{2+}

Prior to any potential measurements, Fe^{2+} sorption isotherms were recorded for goethite, SWy-2, and MX-80 suspensions in duplicate experiments. Each mineral phase was equilibrated with variable concentrations of Fe^{2+} in absence of oxygen inside the glovebox. pH values and solid mass were varied in series of batch experiments that were carried out simultaneously.

Mixed-phase experiments at constant total Fe^{2+}-concentration were carried out as follows.

100 mL of a 1mM Fe^{2+} stock solution was pre-equilibrated with either a clay mineral (0.1 g L^{-1} during 4 h) or with goethite (0.5 g L^{-1} during 24 h). Subsequently, 4 to 6 batch reactors were filled with 12 mL of this suspensions and different amounts of the second solid phase was added and allowed to equilibrate. Finally, 150 µM of mediator, typically ZwiV or CMV, were added to facilitate an electron transfer between the Fe^{2+}/mineral phase system and the electrode. The reduction potential and the pH value of a suspension containing one or several solid phases in equilibrium with dissolved Fe^{2+} was measured using a Pt ring electrode (Metrohm, Switzerland) not earlier than 2 hours after addition of the mediator.

3 Results and Discussion

3.1 Mediated electrochemical reduction and oxidation of reference clay minerals

Mediated electrochemical reduction (MER) and mediated electrochemical oxidation (MEO) are performed to quantify the number of electrons transferred to or from structural Fe in clay suspensions at an applied potential (E_H). The principle outcome of a MER and MEO experiment is illustrated in Fig. 3. At an applied potential E_H of -0.41 neither the addition of native SWa-1 (containing 12.6 wt.-% of Fe^{3+}) nor its dithionite-reduced form (12.3 wt.-% Fe^{2+} after 2 and 20 minutes generated any current responses (see arrows in Fig. 3). This observation demonstrated that direct (i.e., non-mediated) electron transfer between structural Fe and the working electrode either did not occur or was too slow for detection within the timescale of the experiment.

Addition of oxidized diquat (DQ^{2+}) as electron transfer mediator resulted in a sharp (up-ward) reductive current peak (Fig. 3). After an additional 20 min, the current returned to the background value (≈ 10 µA, likely due to minor H^+ reduction), indicating that the diquat redox couple had reached redox equilibrium with the WE. In this kind of experiments, the mediator current peak was integrated as in eq. 1 to confirm that the extent of mediator reduction agreed quantitatively with the value calculated at the applied E_H using the Nernst equation.

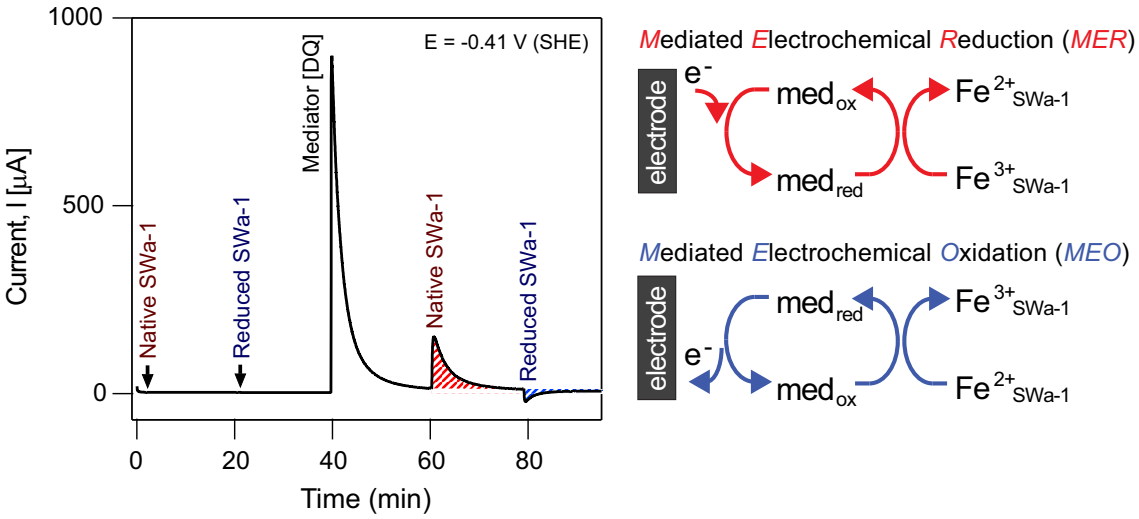

Fig. 3: MER and MEO experiments in an electrochemical cell at pH = 7.5 and at applied E_H = -0.41 V.

Each SWa-1 spike amounted to 370 µg (0.83 µmol) of structural Fe (reproduced with permission from Gorski et al. (2012b), Copyright (2012) American Chemical Society).

In the presence of diquat, addition of native SWa-1 at ca. 60 minutes resulted in a sharp reductive current peak (red shaded area in Fig. 3), whereas an oxidative peak (blue shaded area) was detected upon addition of dithionite-reduced SWa-1 (80 min). Apparently, the electron transfer mediator diquat facilitated electron transfer from the electrode to structural Fe^{3+} as well as from Fe^{2+} in the dithionite-reduced SWa-1 to the working electrode. At the intermediate E_H-

value chosen, both reduction and oxidation of structural Fe in SWa-1 occurred indicating that more extreme reduction potentials are required to quantify the total electron accepting and donating capacities.

3.2 Electron accepting and donating capacities

The electron accepting and donating capacities, Q_{EAC} and Q_{EDC}, of SWa-1, SWy-2, and MX-80 were determined in mol_e-/$g_{clay\ mineral}$ according to procedures similar to the one outlined in Section 3.1. The experiments differed from the previous ones in that strongly reducing (E_H = 0.60 V) and strongly oxidizing (E_H = +0.61 V) potentials were applied to the WE, requiring mediators with different E_H^0-values near the applied E_H. We chose triquat (E_H^0 = -0.54 V) and ABTS (E_H^0 = +0.70 V) for reducing and oxidizing conditions, respectively, to maximize Q_{EAC} and Q_{EDC} values. Both Q_{EAC} and Q_{EDC} were measured by spiking increasing masses of clay mineral to a cell that was pre-equilibrated with the mediator at the one of the defined potentials. Current peaks were integrated by using eq. 1 to determine the number of electrons transferred from the WE to the clay mineral. The results for SWa-1, SWy-2, and MX-80 are shown in Tab. 5.

Tab. 5: Electron accepting and donating capacities of native (nat) and dithionite-reduced (red) clay minerals in mol_e-/$g_{clay\ mineral}$*.

Solid	Redox treatment	Q_{EAC}	Q_{EDC}	Q_{tot}	%-redox-active Fe
SWa-1	Native Reduced	2.21 ± 0.01 0.05 ± 0.01	0 2.24 ± 0.02	2.21 ± 0.01 2.29 ± 0.01	98 ± 1 101 ± 2
SWy-2	Native Reduced	0.40 ± 0.04 0	0 0.39 ± 0.01	0.40 ± 0.04 0.39 ± 0.01	97 ± 14 95 ± 10
MX-80	Native Reduced	0.31 ± 0.01 n.a.**	0.05 ± 0.01 0.39 ± 0.06	0.36 ± 0.02** 0.39 ± 0.06	83 ± 3*** 91 ± 13

* Uncertainties correspond to ± 1 σ
** Includes Fe^{2+} present in native state.
*** n.a. = not applicable; lowest E_H sampled was -0.31 V.

The Q_{EAC}-values of SWa-1 corresponded to 2.21 mol_e-/$g_{clay\ mineral}$ while no electron donating capacity was found in agreement with the observation that all Fe in the native mineral is present as Fe^{3+}. The total electron transfer capacity, Q_{tot}, derived from the sum of electrons transferred at E_H-values of -0.6 and +0.61 V indicated that all Fe^{3+} in the native mineral structure was redox-active. Q_{EAC} -values of dithionite-reduced SWa-1 were negligible compared to Q_{EDC} of 2.24 mol_e-/$g_{clay\ mineral}$. The Q_{tot}-value was similar to the one of native SWa-1 and confirmed that all Fe was redox-active. Moreover, this agreement indicates that negligible (< 1 %) reductive dissolution of Fe^{2+} occurred during the dithionite reduction step.

Analysis of the electron donating and accepting capacities of SWy-2 showed a qualitatively identical behaviour. The Q_{tot}-values of SWy-2 corresponded to on fifth of that of SWa-1 in agreement with the five times higher Fe-content in the latter (Tab. 1). The results for the two source clay minerals, as well as additional ones investigated in Gorski et al. (2012b), show that MER and MEO are a robust approach to quantify directly the electron accepting and donating capacities of smectite clay minerals and discriminate between total Fe contents and redox-active Fe measured by acid dissolution.

A first evaluation of Q_{EAC} and Q_{EDC} of native MX-80 reveals considerable electron accepting and donating capacities, that is 0.31 and 0.05 ge/$g_{clay\ mineral}$, respectively. This result likely reflects the mineralogical composition of MX-80 bentonite, which contains approximately 75 wt.-% of Wyoming montmorillonite, 0.3 wt.-% pyrite, and 0.7 wt.-% siderite. We tentatively attribute the electron accepting capacity to the montmorillonite given that $Q_{EAC}^{MX-80}$is indeed 75 % of Q_{EAC}^{SWy-2}. Moreover, Fe^{2+} sulfides and carbonates could have caused the MX-80 to oxidize at E_H-values of +0.6 V. Despite this good agreement, the above numbers need to be interpreted with caution. Mineralogical analyses of MX-80 showed significant variability with regard to both mineral and elemental composition (Gailhanou et al. 2007, Hunter et al. 2007, Karnland et al. 2006, Madsen 1998, Milodowski et al. 2009a, Milodowski et al. 2009b) and neither mineral nor elemental analyses have been performed in this study to confirm this interpretation.

3.3 Redox profiles as indicators of clay mineral redox properties

Using a selection of electron transfer mediators from Tab. 4, we performed combinations of MER and MEO experiments in the range of E_H-values used for quantification of electron donating and accepting capacities (-0.6 to +0.6 V). Each single MER/MEO experiment contributed a data point from several replicate spikes of clay mineral suspension to the electrochemical cell at a defined E_H in the presence of a mediator. The curve that is produced from plotting the collective MER/MEO results is referred to here as a redox profile. Based on such redox profiles obtained, the redox properties of Fe in SWa-1, SWy-2, and MX-80 could be characterized.

3.3.1 Ferruginous smectite SWa-1

Redox profiles were collected for native, reduced, re-oxidized, re-reduced, and re-re-oxidized SWa-1 samples and are shown in Fig. 4. The redox profiles of the native and reduced SWa-1 samples both illustrate redox activity over wide E_H-ranges, that is 0.4 V for the native and 1.2 V for the reduced SWa-1. These ranges were much wider than expected if the Fe^{2+}/Fe^{3+} redox couple followed Nernstian behaviour (i.e., 99 % reduced to 99 % oxidized from E_0 -0.12 V to E_H^0 +0.12 V). In addition, the redox profiles of native and reduced SWa-1 did not fall onto a single curve but showed obvious path-dependence; the Fe^{2+} content of a sample at a set E_H-value clearly depended on the initial oxidation state of Fe. This observation contradicts a fully reversible electron transfer to and from SWa-1 because the redox profiles would otherwise have fallen onto one curve. Notice that kinetic artifacts can be ruled out (see detailed discussion in Gorski et al. 2012c).

The observed path-dependence in the SWa-1 redox profiles was therefore attributed to the reduction and oxidation of SWa-1 being thermodynamically irreversible, with at least one of the redox envelopes not representing thermodynamic equilibrium. One possible origin of the thermodynamic irreversibility was that the dithionite reduction step and/or the electrochemical re-oxidation caused a permanent change in the mineral structure that affected the coordination environment of structural Fe and thus, its reduction potential. This would have resulted in the reduction of native SWa-1 and the oxidation of reduced SWa-1 being distinct reactions. This type of redox reaction is said to be chemically irreversible (Bard & Faulkner 2001b).

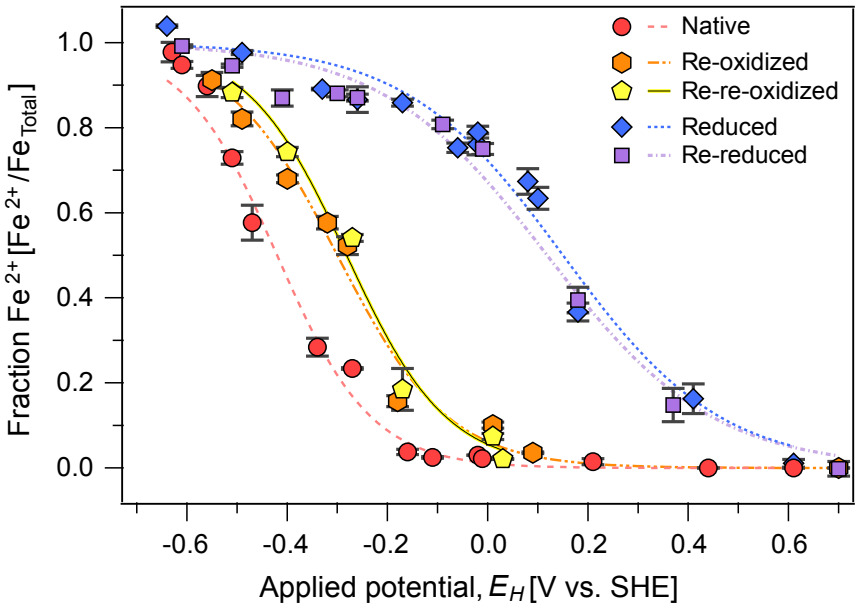

Fig. 4: Redox profiles of native and several, redox-cycled ferruginous smectite suspension.

(SWa-1, reproduced with permission from Gorski et al. (2012c), Copyright (2012) American Chemical Society).

Effect of redox cycling on SWa-1 redox profiles

Extensive redox cycling of SWa-1 revealed that collectively, redox profiles could be grouped as *native, oxidized,* and *reduced* because re-oxidized and re-re-oxidized, and reduced and re-reduced samples behaved almost identically (Fig. 4). The difference between the native and re-oxidized redox profiles was consistent with two specimens being chemically dissimilar, and thus the reduction of native SWa-1 and the subsequent re-oxidation of reduced SWa-1 were chemically irreversible. This observation was in good agreement with spectroscopic studies that have shown structural changes that occur as a result of reduction and re-oxidation of Fe-bearing smectites (Anastacio et al. 2008, Fialips et al. 2002a, Fialips et al. 2002b, Komadel et al. 1995, Manceau et al. 2000a, Neumann et al. 2011a, Rozenson & Heller-Kallai 1976). Collectively, these studies indicate that reduction and subsequent re-oxidation of clay minerals results in a net loss of structural hydroxyl groups, increased structural disorder of the Fe atoms, and partial migration of Fe atoms within the octahedral sheet from cis-octahedral sites (i.e., two adjacent binding hydroxyl groups) to *trans*-octahedral sites (i.e., two binding hydroxyl groups opposite one another), which is coupled to the mobilization of Fe from dioctahedral domains (where approximately one-third of octahedral sites are vacant) to trioctahedral domains (where all octahedral sites are occupied within a cluster). These changes likely alter the redox properties of structural Fe. Note that because dithionite was used almost exclusively as the reductant in previous studies (Anastacio et al. 2008, Fialips et al. 2002a, Fialips et al. 2002b, Komadel et al. 1995, Manceau et al. 2000a, Neumann et al. 2011a, Rozenson & Heller-Kallai 1976), it remains unclear whether these structural changes observed are specific to reduction by dithionite or if they occur when other chemicals or microorganisms are used as the reductant (Lee et al. 2006, Stucki et al. 1996).

Further redox cycling beyond the first re-oxidation step showed that the redox profile path dependence persisted (Fig. 4). The re-reduced SWa-1 redox profile was indistinguishable from the reduced SWa-1 redox profile, and the re-re-oxidized SWa-1 redox profile was indistinguishable to the re-oxidized SWa-1 redox profile. These similarities suggested that after the first reduction and re-oxidation cycle, no further chemically irreversible structural changes occurred, but SWa-1 reduction and oxidation remained thermodynamically irreversible.

3.3.2 Wyoming montmorillonite SWy-2

The redox profile of native SWy-2 together with reduced, re-oxidized, and re-reduced specimen is shown in Fig. 5. As was found for the native SWa-1, the extent of Fe^{3+}-reduction increases with decreasing E_H. Once E_H is sufficiently low, all structural Fe^{3+} was reduced consistent with Q_{EAC} -determination. Structural Fe^{3+} in SWy-2 was reduced at much higher E_H-values than Fe^{3+} in SWa-1. This effect can be attributed to SWy-2 having lower Fe content (2.3 wt.-%, Tab. 1). Native SWy-2 was redox-active over a larger E_H-range (≈ 0.8 V) compared to native SWa-1 (≈ 0.5 V), an effect that is currently difficult to rationalize. In contrast to SWa-1, SWy-2 lacks a high enough structural Fe content that would enable octahedral Fe sites that exhibit interdependent redox activities or multiple Fe sites due to different next-nearest neighbours (Neumann et al. 2011a) This spectroscopic evidence is in agreement with the redox profiles observed for reduced, re-oxidized, and re-reduced specimen of SWy-2. Path-dependence was relatively minor as compared to SWa-1 as would be expected by the low Fe content and lack of irreversible structural Fe re-arrangements upon electron transfers to and from the clay mineral.

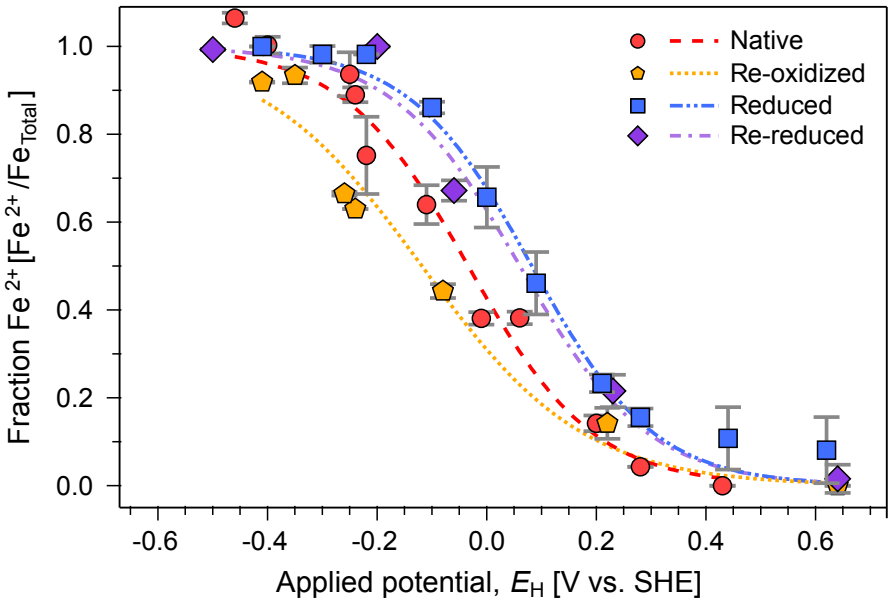

Fig. 5: Redox profile of native, oxidized (re-oxidized), and reduced (incl. re-reduced) SWy-2 (reprinted from Gorski et al. 2013).

3.3.3 MX-80 bentonite

Redox profiles of a native, reduced and re-oxidized MX-80 are shown in Fig. 6. Native material contained approximately 0.3 wt.-% residual Fe^{2+} (of 2.4 wt.-% Fe_{tot}) even when exposed to air. This number can tentatively be linked to the Fe^{2+}-minerals other than smectites (e.g., siderite and pyrite, see Karnland et al. 2006). 72 % of the total structural Fe in the native MX-80 was reduced at E_H of -0.55 V, while 10 – 12 % of the total structural iron was oxidized at E_H = +0.64 V in the same samples. Thus, up to 85 % of the total Fe was found redox-active in the E_H range -0.55 to +0.64 V did not count 100 %.

The redox profile exhibited similar shape as the one of SWy-2, most likely reflecting the montmorillonite content of MX-80. As found for SWy-2, dithionite-reduced MX-80 showed a redox profile that resembled that of the native specimen. The data in Fig. 6, however, scatter more than in experiments with purified source clay minerals. Whether the experimental variability is due to the limited amount of experiments or heterogeneity of the material analysed cannot be answered conclusively here. It is interesting to note that the fraction of residual Fe^{2+} did not disappear completely when the dithionite-reduced specimen were equilibrated at E_H of +0.64 V but, again, the uncertainty of this measurement is relatively large. This fraction of structural Fe^{2+} is preserved even after re-oxidation of reduced MX-80 with H_2O_2 and the redox profile of the re-oxidized sample follow that of the native sample. This observation is supports the hypothesis that the redox properties of MX-80 are determined by its montmorillonite fraction and thus follows the same trends as found for SWy-2.

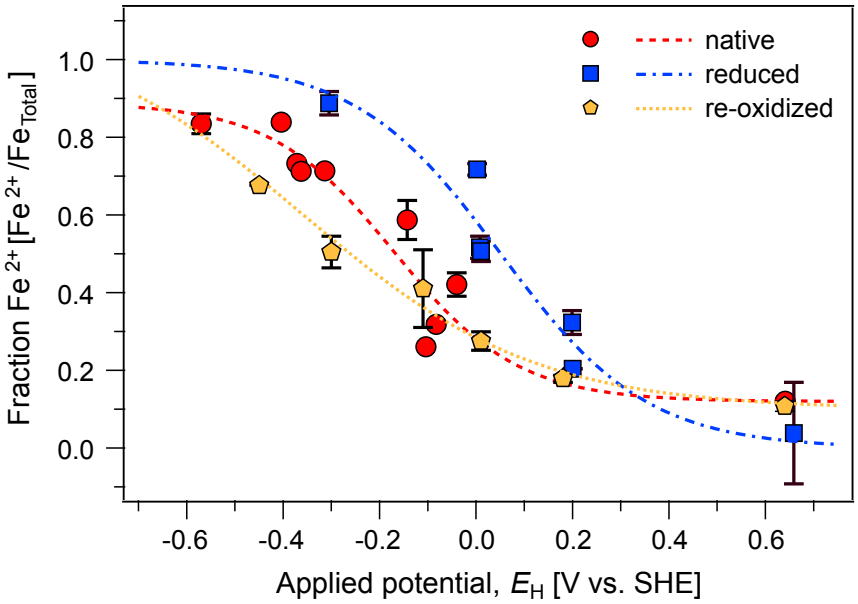

Fig. 6: Redox profiles of the native, re-oxidized and reduced MX-80.

3.4 Spectroscopic characterization of redox-cycled SWa-1

X-ray absorption and Mössbauer spectroscopy of native and redox-cycled SWa-1 was carried out to obtain evidence for structural changes in the local Fe coordination environment that might have accompanied Fe^{3+} reduction and Fe^{2+} re-oxidation. Spectroscopic observations were interpreted with regard to the distinct electrochemical behaviour of native, oxidized, and reduced samples.

3.4.1 XAS characterization of redox-cycled SWa-1

We examined redox-cycled SWa-1 samples using Fe K-edge X-ray absorption near-edge structure (XANES) and extended X-ray absorption fine structure (EXAFS) spectroscopy. In the XANES spectra, the absorption edge of the *reduced* SWa-1 is located at an energy lower than that of the edge position of the *native* SWa-1 due to Fe^{2+} having an electron binding energy lower than that of Fe^{3+} (Fig. 7a). Differences between the native and *reduced* SWa-1 were also observed in their EXAFS spectra in *k*-space (Fig. 7e) and *R*-space (Fig. 7f).

To gain quantitative information regarding the local Fe coordination in reduced SWa-1, the first-shell Fe-O_1 peak (A) was evaluated by shell-fitting (details in Gorski et al. 2012c). The fitting results indicated an increase in the Fe-O distance from ≈ 2.01 Å in the *native* to ≈ 2.10 Å in the *reduced* SWa-1. The *reduced* SWa-1 spectrum exhibited a first-shell amplitude (peak A intensity) lower than that of the native SWa-1, which was attributed to a larger spread in Fe-O1 distances (Manceau et al. 2000a). Peaks C and F were only present in the *reduced* SWa-1 spectrum. These peaks have been attributed to out-of-plane oxygen contributions (Fe-O3, peak C) and a third Fe shell in collinear arrangement (Fe-Fe3, peak F) and have been suggested to indicate the formation of trioctahedral domains (Manceau et al. 2000a).

Little difference was observed between the XANES spectra of the *native, re-oxidized, re-re-oxidized* SWa-1 (Fig. 7d). The EXAFS spectra, however, showed significant differences between the *native* and *re-oxidized* samples (Fig. 7e). In the EXAFS spectra of *re-oxidized* and *re-re-oxidized* SWa-1 the first-shell (Fe-O_1 bond) intensity decreased (peak at ≈ 1.5 Å), which was attributed to an increased distortion in the Fe^{3+}-octahedra (Gates et al. 2002, Manceau et al. 2000a). Fits of the first shell showed that the average first shell Fe-O_1 distance did not change from the native to the *re-oxidized* SWa-1 but returned a lower coordination number and higher Debye-Waller factor for the re-oxidized sample, suggesting an increase in octahedral distortion (Gorski et al. 2012c). No further change(s) in the EXAFS spectra were observed between the *re-oxidized* and *re-re-oxidized* SWa-1 (Fig. 7c). Nearly identical XANES and EXAFS spectra were also observed for the *reduced* and *re-reduced* SWa-1 (Fig. 7e). These results are in good agreement with the hypothesis that only the first redox-cycle caused irreversible structural changes. The spectral changes observed between the *native* and *re-oxidized* SWa-1 (Fig. 7c) coupled with the MER and MEO redox profiles (Fig. 4) indicated that the increased distortion in the Fe^{3+}-octahedra is linked to re-oxidized SWa-1 being reduced at more positive E_H-values than native SWa-1.

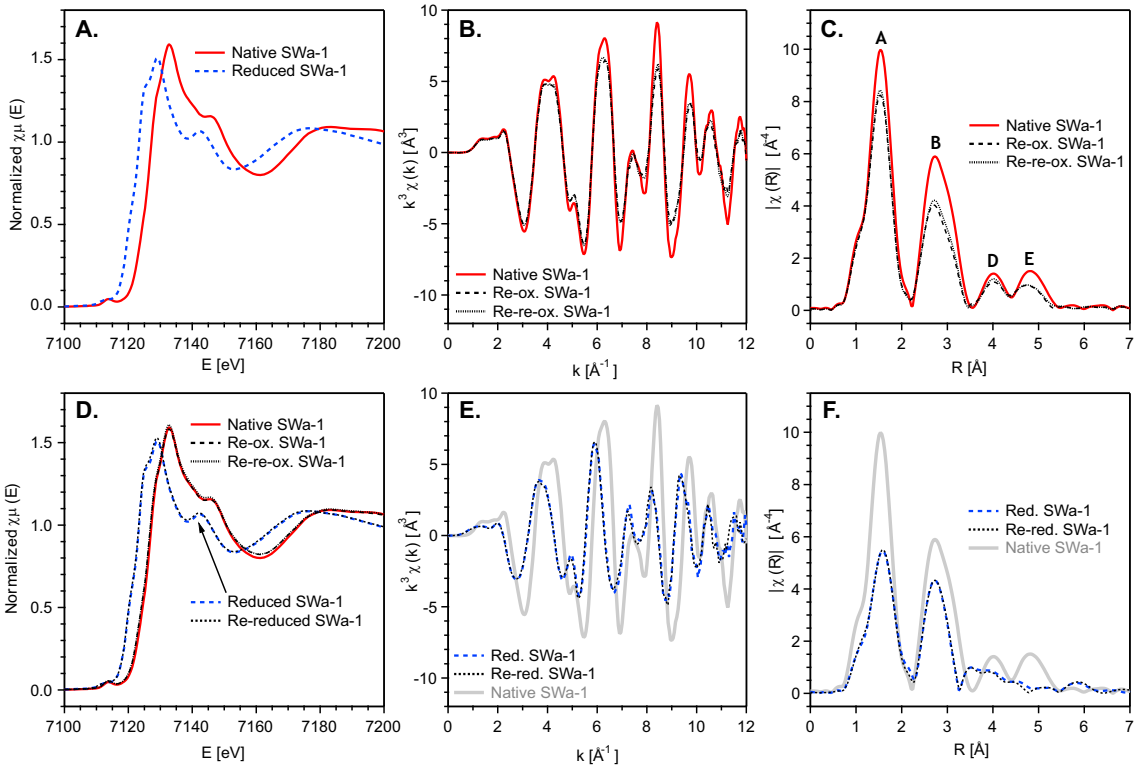

Fig. 7: (a) Fe K-edge XANES spectra of native and dithionite reduced SWa-1, (b) EXAFS spectra in *k*-space of native, re-oxidized and re-re-oxidized SWa-1, (c) Fourier-transform magnitude of the EXAFS spectra of native re-oxidized and re-re-oxidized SWa-1, (d) Fe K-edge XANES spectra of native, reduced, re-oxidized, re-reduced, and re-re-oxidized SWa-1, (e) EXAFS spectra in *k*-space of native, re-reduced, and re-re-reduced SWa-1, (f) Fourier-transform magnitude of the EXAFS spectra of native, re-reduced, and re-re-reduced SWa-1.

Peak naming is consistent with Manceau et al. (Manceau et al. 2000a) [A] nearest O shell, Fe-O_1; [B] combined contributions from the nearest octahedral Fe or Al shells Fe (Fe-Fe_1, Fe-Al_1), the nearest tetrahedral Si or Al (Fe-Si_1, Fe-Al_1), and the next-nearest O shells (Fe-O_2); [C] the third nearest O shell (Fe-O_3); [D] next nearest tetrahedral Si or Al (Fe-Si_2, Fe-Al_2); [E] next-nearest octahedral Fe or Al shells (Fe-Fe_2, Fe-Al_2); [F] the third nearest octahedral Fe or Al shells (Fe-Fe_3, Fe-Al_3).

3.4.2 Mössbauer spectroscopy

Mössbauer spectra were also collected for the native, re-oxidized, and re-re-oxidized samples (8). The native SWa-1 spectrum was typical for structural Fe^{3+} in a clay mineral (Dyar 1987) and could be modelled with a single octahedral (Oct) Fe^{3+} site (8, top; center shift (CS) = 0.44 mm/s, quadrupole splitting (QS) = 0.00 mm/s). This spectrum is very similar to a previously published spectrum of SWa-1 (Dyar 1987). Because the spectrum contained a singlet peak (i.e., QS ≈ 0 mm/s), the Fe^{3+} was further characterized as cis-octahedral Fe^{3+} (i.e., two adjacent binding hydroxyl groups), as opposed to trans-octahedral Fe^{3+} (i.e., two hydroxyls opposite each other), which would have had a larger QS value (≈ 0.7 - 1.0 mm/s) (Dyar 1987) and would manifest as a doublet (i.e., two separate peaks).

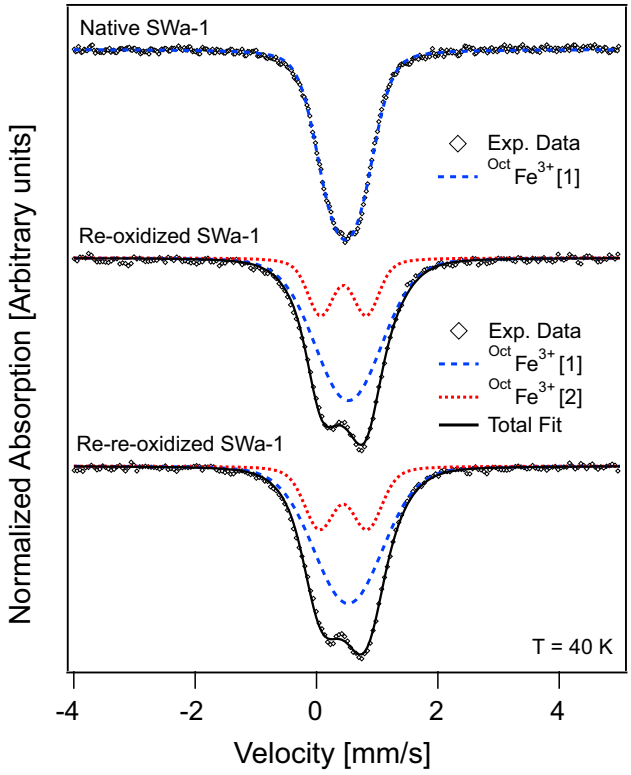

Fig. 8: ^{57}Fe Mössbauer spectra of purified and size-fractionated *native* and *oxidized* SWa-1 collected at 13 K.

Reproduced with permission from Gorski et al. 2012c, Copyright (2012) American Chemical Society).

Spectra were modelled using Voigt-based fitting (Rancourt & Ping 1991). Hyperfine parameters from the fits see Gorski et al. (2012c).

The spectrum of *re-oxidized* SWa-1 was substantially different from that of the *native* SWa-1; the singlet split into a doublet and the spectrum became asymmetric (8, middle). The spectrum was best modelled with two Fe^{3+} sites, one very similar to the initial $_{Oct}Fe^{3+}$ site (CS = 0.52 mm/s, QS = 0.00 mm/s, 75 % of spectral area), and the other (25 %) with a similar CS value (0.44 mm/s) and a much larger QS value (0.75 mm/s). The *re-re-oxidized* SWa-1 spectrum was very similar to the re-oxidized SWa-1 spectrum (8, bottom; CS1 = 0.52 mm/s, QS1 = 0.02 mm/s, area1 = 70 %; CS2 = 0.44 mm/s, QS2 = 0.79 mm/s, area2 = 30 %). The formation of a new site with a large QS value was in good agreement with previous studies that observed the appearance of new, large QS site after reduction and re-oxidation of SWa-1 (Komadel et al. 1995) and other clay minerals (Anastacio et al. 2008). An increase in the QS value has previously been linked to structural de-hydroxylation in SWa-1 (Dainyak et al. 2006).

The newly formed phase in the oxidized (i.e., re-oxidized and re-re-oxidized) spectra with a large QS value has been previously interpreted as both distorted *cis*-octahedral Fe^{3+} (Besson et al. 1983, Cashion et al. 2010, Cashion et al. 2008, Goodman et al. 1976, Russell et al. 1979) and transoctahedral Fe^{3+} (Jaisi et al. 2009, Jaisi et al. 2005, Luca 1991). Regardless of the exact structural coordination of this Fe phase, the formation of this new phase can be linked to reduction of *oxidized* SWa-1 occurring at more positive E_H-values than for native SWa-1. This observation is consistent with previous studies that observed structural Fe^{3+} in nontronites with a

larger QS value was preferentially reduced over structural Fe^{3+} with smaller QS values (Jaisi et al. 2009, Jaisi et al. 2005, Schaefer et al. 2011). As a result, QS values may be indicative of what E_H-value(s) are required to reduce structural Fe^{3+} in a clay mineral.

3.4.3 Quantification of apparent reduction potentials ($E_H^{\emptyset}$)

Based on the spectroscopic and electrochemical evidence gathered for SWa-1, we conclude that different groups exist with different structural and redox properties: e.g. native, oxidized (i.e., re-oxidized and re-re-oxidized), and reduced (i.e., reduced, and re-reduced). Because a system at thermodynamic equilibrium can only have a single redox profile at least two of three redox profiles of SWa-1 must reflect metastable states. To relate the extent of Fe^{3+}-reduction to E_H-values, we introduce apparent standard reduction potentials ($E_H^{\emptyset}$), which allow for metastability and thus differ from true standard reduction potentials (i.e. E_H^0).

For samples containing an indefinite number of sites or interdependent redox-active moieties, a modified Nernst equation has been used that includes an additional parameter (β) that accounts for wider distributions (eq. 3) (Castro et al. 1996):

$$E = E_H^{\emptyset} - \frac{1}{\beta} \text{ x } \frac{RT}{nF} In \frac{[Fe^{2+}]}{[Fe^{3+}]}$$

where R, T, n and F have their usual meanings and β is a unit less, fractional value ($0 < \beta < 1$), with wider distributions resulting in smaller β values, and $[Fe^{2+}]$ and $[Fe^{3+}]$ reflect the content of different redox-active Fe species. Inclusion of the β term is mathematically equivalent to creating a continuous uniform distribution of E_H^0-values. As shown in Fig. 4, 5, and 6, the model accurately fits all redox profiles and the results are shown in Tab. 6.

SWa-1

Similar to what we observed qualitatively and spectroscopically for SWa-1, the fitted $E_H^{\emptyset}$ and β values for the redox profiles clustered into three groups: native, oxidized, and reduced. Thus, the difference in $E_H^{\emptyset}$-values between the native and reduced SWa-1($\Delta E_H^{\emptyset}$ = 0.53 V) and oxidized and reduced SWa-1 ($\Delta E_H^{\emptyset}$ = 0.43 V) reflected a strong path dependence (i.e., thermodynamic irreversibility) in the reduction and oxidation of SWa-1. We attribute the observed widened potential distributions reflected in β values between 0.16 and 0.30 to SWa-1 containing multiple types of reactive sites and/or the reactive sites exhibiting interdependent reactivities. The β values fitted for these samples varied considerably between the native (0.30), oxidized (0.25), and reduced (0.16) SWa-1. We hypothesize that smaller β values for the reduced SWa-1 indicated that interactions between neighboring Fe atoms were more pronounced in these samples than for the native and oxidized samples, and thus reduced SWa-1 showed the most substantial derivation from Nernstian behaviour. This observation is consistent with EXAFS spectra of the reduced SWa-1 containing evidence for the presence of trioctahedral domains and previous work showing increased Fe-Fe interactions in reduced SWa-1 using infrared (IR) spectroscopy (Komadel et al. 1995, Neumann et al. 2011a).

Using eq. 3, we calculated an operational E_H-range, in which SWa-1 would be expected to buffer the reduction potential. To this end, we derived the $E_H^{\emptyset\dagger}$-values at which 90 % of Fe in SWa-1 was reduced or oxidized, respectively. As shown by the $E_H^{\emptyset\dagger}$-values in Tab. 3, differ from the $E_H^{\emptyset}$ by ±130 to ±300 mV. This numbers imply that the different redox-modified species of SWa-1 would buffer the reduction potential over a more than 2-fold range compared to Fe^{2+}/Fe^{3+}-redox couple following a Nernstian relationship (±56 mV).

SWy-2

Identical analyses were carried out with the redox profiles of SWy-2. In agreement with earlier observations that chemically reduced montmorillonites not as good a reductant of organic compounds than SWa-1 (Hofstetter et al. 2006, Neumann et al. 2008), $E_H^{\emptyset}$-values are indeed higher by 380 mV if native clay minerals are compared while the difference is only 40 mV for the reduced specimen. A higher apparent reduction potential of SWy-2 can be rationalized with its lower structural Fe content and Fe present in isolated, ordered entities in the octahedral sheet lacking the ability to from reactive Fe-clusters (Vantelon et al. 2003). A lack of substantial structural changes would confirm a minor extent of hysteresis observed in the redox profiles of native, re-oxidized, and reduced SWa-1. Notice that the much lower $E_H^{\emptyset}$ of the re-oxidized specimen can also be due to experimental uncertainty (Fig. 5). However, β-values for SWy-2 are in a similar range as for SWa-1 and indicate the same extent of deviation from the Nernst equation even though IR-spectroscopic work showed that SWy-2-reduction and re-oxidation was characterized by little octahedral distortion (Neumann et al. 2011a). It is currently unclear why SWy-2 would buffer the redox potential over such a large range (cf. $E_H^{\emptyset\dagger}$-values in Tab. 6) despite the absence of detectable structural alterations.

Tab. 6: Modelling parameters of the redox profiles: apparent reduction potential, $E_H^{\emptyset}$, and β-values and $E_H^{\emptyset\dagger}$-values at 90 % and 10 % Fe^{2+}-content.

Uncertainties represent 95 % confidence intervals.

Clay mineral	**Redox modification**	$E_H^{\emptyset}$ **vs. SHE** [V]	B [-]	$E_H^{\emptyset\dagger}$ **90 % Fe^{2+}** [V]	$E_H^{\emptyset\dagger}$ **10 % Fe^{2+}** [V]
SWa-1	Native	-0.41 ± 0.01	0.30 ± 0.02	-0.54	-0.28
	Re-oxidized	-0.30 ± 0.01	0.23 ± 0.03	-0.49	-0.11
	Re-re-oxidized	-0.28 ± 0.01	0.26 ± 0.03	-0.44	-0.12
	Reduced	+0.15 ± 0.02	0.16 ± 0.02	-0.15	+0.44
	Re-reduced	+0.12 ± 0.02	0.16 ± 0.02	-0.18	+0.42
SWy-2	Native	-0.03 ± 0.02	0.23 ± 0.03	-0.22	+0.16
	Re-oxidized	-0.12 ± 0.03	0.17 ± 0.03	-0.40	+0.16
	Reduced	+0.08 ± 0.01	0.23 ± 0.02	-0.11	+0.27
MX-80	Native	-0.20 ± 0.03	0.24 ± 0.05	-0.35	-0.02
	Re-oxidized	-0.36 ± 0.02	0.12 ± 0.01	-0.77	+0.05
	Reduced	+0.05 ± 0.02	0.17 ± 0.04	-0.23	+0.33

MX-80 bentonite

$E_H^{\emptyset}$-values for MX-80 only slightly shifted to lower potential values than SWy-2 as implied from the comparison of redox profiles and the montmorillonite content of MX-80. Due to experimental variability, $E_H^{\emptyset}$ vary by 250 mV between native and reduced specimen as opposed to 40 mV difference reported for SWy-2 (Tab. 6). β-values are among the lowest found for the three minerals studied but again agree with the above interpretations and imply that the approach chosen here for the characterization of redox properties is consistent. An explanation for the strong deviation from a Nernstian behaviour, however, could not be found.

3.5 Mixed-phase systems

3.5.1 Redox properties of Fe^{3+}-bearing minerals in the presence of dissolved Fe^{2+}

Current evidence for interfacial electron transfer between adsorbed Fe^{2+} and Fe^{3+} in the structure of various iron oxides (Beard et al. 2010, Gorski et al. 2012a, Gorski & Scherer 2009, Larese-Casanova & Scherer 2007, Latta et al. 2012a, Williams & Scherer 2004) as well as Fe-rich for clay minerals (Schaefer et al. 2011) point to noticeable redox activity of surfacebound Fe. Conceptual models have been proposed to rationalize the phenomenon of Fe^{2+}-adsorption, by electron transfer to solid Fe^{3+} (eqs. 4 and 5) followed by bulk conduction and reductive dissolution (Gorski & Scherer 2011).

$$\equiv Fe^{3+} - OH + Fe^{2+} + H_2O \leftrightarrow \equiv Fe^{3+} - O - Fe^{2+} - OH + 2\ H^+ \quad (4)$$

$$\equiv Fe^{3+} - O - Fe^{2+} - OH \rightarrow \equiv Fe^{2+} - O - Fe^{3+} - OH \quad (5)$$

There is, however, only little evidence for the reduction potentials, at which these processes happen (Gorski et al. 2010) and no conceptual description of the involved redox-active Fe species. Using a modified electrochemical approach (Chapter 2.6.2) that included electron transfer mediators (CMV and ZwiV, Tab. 4), we assessed the apparent reduction potential of suspensions in the presence of dissolved Fe^{2+}.

Goethite/Fe^{2+}

E_H-values of suspensions containing various amounts of goethite and Fe^{2+} were measured successfully using ZwiV and CMV as ET-mediators over the pH range 6.75 to 7.75 is shown in Fig. 9. While numerous studies report on the reactivity enhancement of Fe-oxide bound Fe^{2+} in comparison to dissolved (aquo)complexes (Hofstetter et al. 1999, Klausen et al. 1995, Liger et al. 1999, Pecher et al. 2002, Silvester et al. 2005), reduction potential of the involved Fe species remained elusive. Theoretical calculations suggested an E_H of -0.2 V at pH 7.0 (Stumm & Sulzberger 1992) but were contrasted by measurements exceeding this value by almost 400 mV (Liger et al. 1999). Because of the multitude of processes affecting the electron transfer from Fe^{2+} associated with Fe oxides (see eqs. 4 – 5) there is no conclusive evidence regarding the redox-active species and processes that would be responsible for the measured potentials.

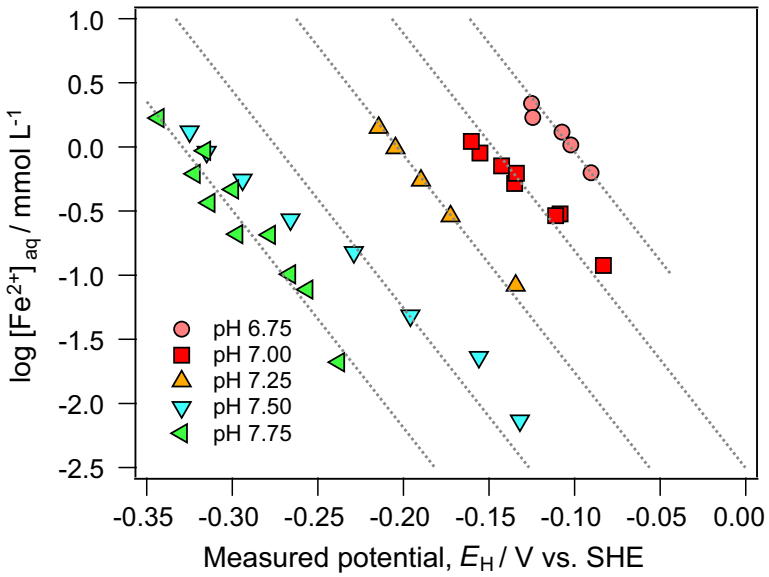

Fig. 9: Fe^{2+} sorption on goethite (1 g/L) at different pH in the range 6.75 – 7.75.

Concentration of dissolved Fe^{2+} was measured 24 h after addition of goethite and 2 h after mediator (ZwiV or CMV) addition to the batches. Lines are representation of a modified Nernst equation with $\beta = 1$.

Our attempt to measure E_H-values in the presence of electron transfer mediators have resulted in a first series of consistent data (Fig. 9) for dissolved Fe^{2+} concentrations between 10 μM and 1.5 mM. Measured E_H covers typical ranges reported for goethite-bound Fe^{2+} from -50 to -350 mV (vs. SHE). An increase in total Fe^{2+}-concentration coincides with an increase of hypothesized, mineral-bound Fe^{2+} and correlates well with lower E_H-values. The goethite mass present in the reactors (0.1 to 2.0 mg L^{-1}), however, did not affect E_H-measurements. Tentative rationalization of the Fe^{2+}-dependent reduction potentials agreed with the reductive dissolution of goethite (eq. 6).

$$\alpha\text{-FeOOH} + 3\ H^+ + e^- \leftrightarrow Fe^{2+} + 2H_2O \qquad (6)$$

The correlation can be assessed the Nernst equation 3 without invoking non-ideal electron transfer behaviour ($\beta = 1$, dashed lines in 9). An increase in solution pH is adequately reflected in decreasing E_H-values consistent with theory (Stumm & Morgan 1996). Tentative rationalization of the pH-dependent reduction potentials suggest a decrease of E_H by The pH-dependence of the measured E_H was -187 mV/pH and suggests a 3:1 H^+/e^--transfer stoichiometry, which is also consistent with eq. 6.

Montmorillonite SWy-2/Fe^{2+}

Similar experiments were performed with SWy-2 suspended in Fe^{2+}-containing batch reactors. An example for a suspension containing fixed total amount of Fe (1 mM) at pH 7.5 is shown in Fig. 10. By varying the amount of clay mineral, up to 90 % of the Fe^{2+} were adsorbed and the E_H were measured. We observed an identical qualitative trend in that larger Fe^{2+} concentrations correlated with lower E_H-values. Notice the influence of the Fe^{3+} phase on the apparent reduction potential. While Fe^{2+} associated with SWy-2 in the presence of 0.75 mM dissolved Fe^{2+} exhibits an apparent E_H of -140 mV, the corresponding dissolved Fe^{2+} concentration in equilibrium with goethite resulted in a substantially lower E_H below -300 mV (Fig. 9).

We also examined the E_H of three pH values, that is, 7.25, 7.5, and 7.75 and modulated the amount of Fe^{2+} as illustrated in Fig. 11. As with goethite/Fe^{2+}-systems, log-linearized E_H-trends were recorded as a function of dissolved Fe^{2+}. In contrast to the latter, trend-lines reflect the behaviour of a modified Nernst-equation with β = 0.31, in which E_H is more sensitive to changes in dissolved Fe^{2+} and pH. The β-value was in the range of those derived from MER/MEO experiments with native SWy-2 (Tab. 6) and led to a reasonable description of the data. Data and trend-lines in Fig. 11 reveal that already a moderate increase of 0.5 pH units is associated with a substantial shift in E_H by -200 mV.

Potential measurements range from -0.05 to -0.3 V and overlap with E_H-ranges of SWy-2 containing 40 – 90 % of reduced structural Fe (Fig. 5). It is thus likely that the redox-active Fe species not only arise from Fe^{2+} associated with clay mineral surfaces but also structural Fe^{2+} as formed from native SWy-2 reduction with dithionite. The latter is supported by the need to adjust the Nernst equation with similar parameters as for redox-modified SWy-2 and observations of interfacial electron transfer from adsorbed Fe^{2+} on different nontronites (Neumann et al. 2013, Schaefer et al. 2011).

3.5.2 Redox properties of binary mineral-phase systems

The characterization of redox properties of the mixed phase system involved experiments, in which goethite or a clay mineral was exposed to dissolved Fe^{2+} before a second mineral phase, that is a clay mineral or goethite was added. Clay minerals used were either SWy-2 or MX-80 bentonite. Experiments were carried out at pH 7.50 and with a fixed total Fe^{2+} concentration of 1.0 mM (Tab. 2). Changes in dissolved Fe^{2+} were achieved by increasing the mass of the second phase added.

Goethite/SWy-2/Fe^{2+}

Fig. 12a shows the the E_H vs. the log of the dissolved Fe^{2+} concentration from four experiments. Those with either goethite/Fe^{2+} and SWy-2/Fe^{2+} display the identical data from Figs. 9 and 11. Regardless of the addition of either SWy-2 to goethite/Fe^{2+} or goethite to SWy-2/Fe^{2+} suspension, we obtained the identical correlation of E_H and dissolved Fe^{2+} concentration. This result shows that potentiometric measurements were at equilibrium and no Fe^{2+}-induced phase transformations occurred that would have altered the measured E_H-values.

There is also a noticeable overlap between data points obtained in suspensions of goethite/Fe^{2+} with and without SWy-2 suggesting that the presence of a clay mineral did not modulate the apparent E_H-value of the suspension as for Fe^{2+}-concentrations below approximately 1 mM. While Fe^{2+} is clearly present at the surfaces of SWy-2, any Fe species formed from interactions of surface bound and dissolved Fe^{2+} with structural Fe^{3+} did not contribute the buffering the E_H. Under the chosen experimental conditions, in which both minerals were present in identical masses but contributed different amounts of structural Fe, we can therefore conclude that the roles of the Fe oxide and the clay mineral were fundamentally different with regard to the suspensions's redox properties. While SWy-2 seem to act primarily as a sorbent for Fe^{2+}, Fe^{2+}-Fe^{3+}-interaction at goethite surfaces determine the system EH. We hypothesize that contributions of Fe^{2+}-clay mineral interactions will become more important as the amount of structural Fe in the clay mineral approaches that of Fe in goethite.

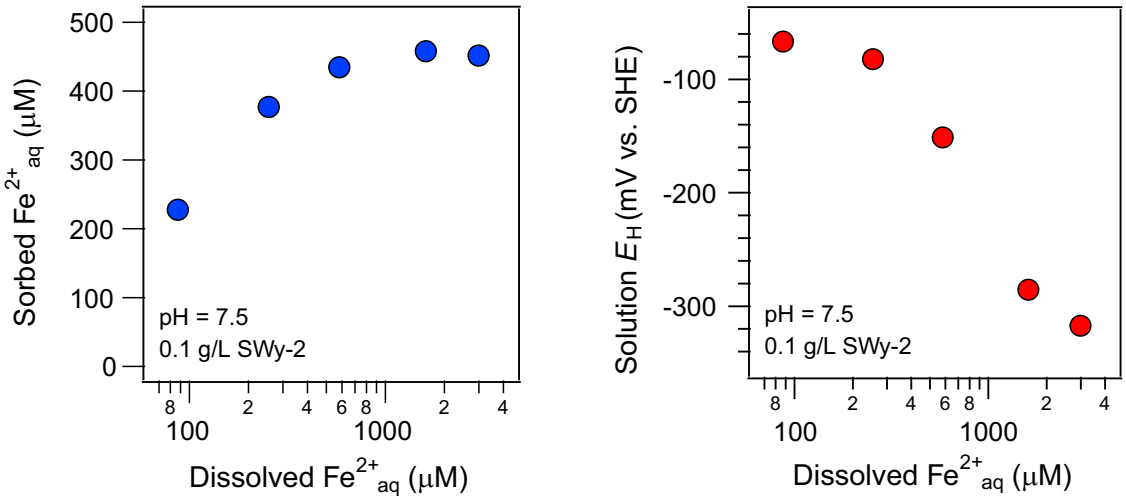

Fig. 10: Left panel: Fe^{2+} sorption on SWy-2 at pH 7.5 and 1 mM total Fe^{2+}.
Right panel: corresponding E_H-values measured in suspension.

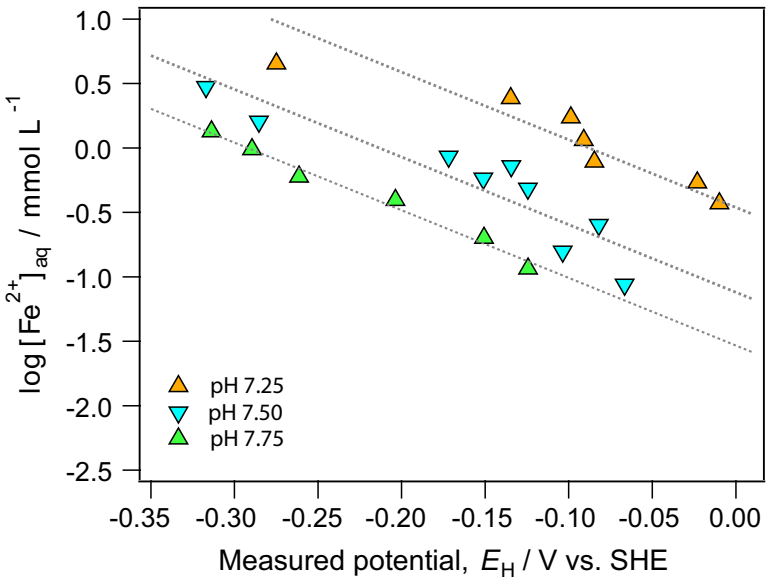

Fig. 11 Fe^{2+} sorption on SWy-2 (0.1 g/L) at pH = 7.5.
Trend-lines represent fits with eq. 3 using a β of 0.31.

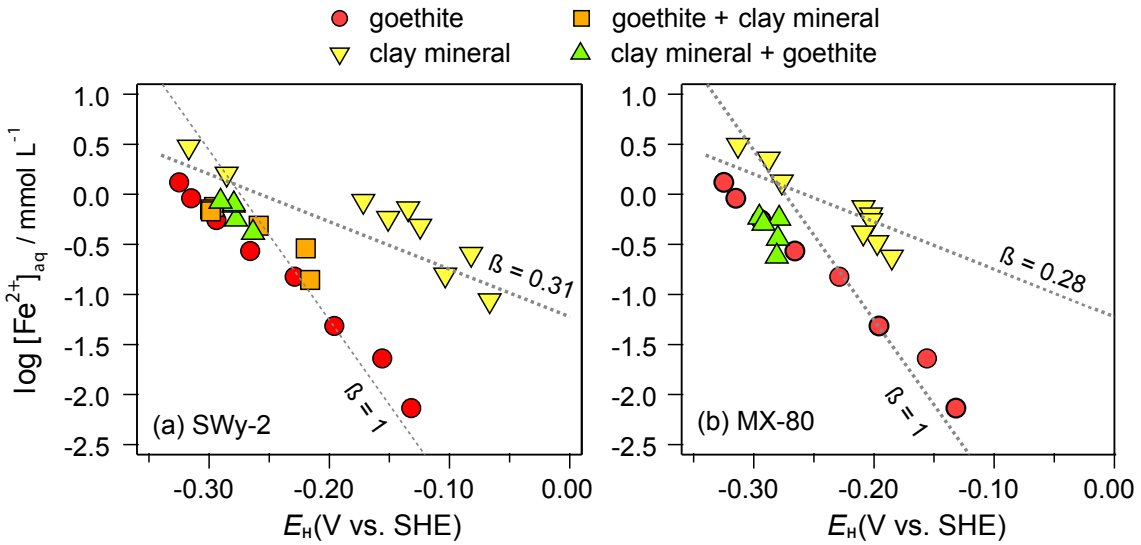

Fig. 12: Fe^{2+} sorption on 1 g/L goethite (red circles), 0.1 g/L clay mineral (yellow squares) or on the mixed phase: 0.5 g/L goethite and 0.5 g/L SWy-2 (a) or (b) MX-80.

Initial dissolved Fe^{2+} in batches was 1 mM, pH = 7.5. Lines are representations of a modified Nernst equation with $\beta = 1$ for goethite, $\beta = 0.31$ for SWy-2, and $\beta = 0.28$ for MX-80.

Goethite/MX-80/Fe^{2+}

The identical mixed phase experiment was carried out with MX-80 bentonite instead of SWy-2 and the results are shown Fig. 12b. In this case, goethite was added to MX-80/Fe^{2+}-suspensions. As reported for comparison of redox properties of SWy-2 vs. MX-80, both clay minerals behaved almost identically, that is Fe^{2+} associated with goethite leads to the formation of EH-determining species while MX-80 acts as sorbent and thus determines the amount of Fe^{2+} that can interact with goethite.

4 Implications

The present work illustrates that mediated electrochemical analyses offers a very promising approach to determine the redox properties of Fe-bearing minerals as well as complex mixed phase systems, in which redox-active Fe is present in a variety of different chemical species.

The redox properties determined for a selection of clay minerals and MX-80 using MER/MEO reveal that structural Fe can in fact buffer the E_H over an enormous potential range. The evidence from this work is compiled in Fig. 13, in which reduction potentials of several contaminants and geochemical redox couples are compared to the $E_H^{\emptyset}$ of SWa-1, SWy-2, MX-80, and Fe^{2+}-mixed phase systems. The wide potential distribution reported here is primarily due to the strong hysteresis of redox properties induced by structural alterations of Fe redox reactions. This rather special redox behaviour of Fe-bearing clay minerals suggest that despite a low Fe content compared to Fe oxides, structural Fe in clay minerals can, for a thermodynamic perspective, participate in many redox processes of biological and geochemical relevance.

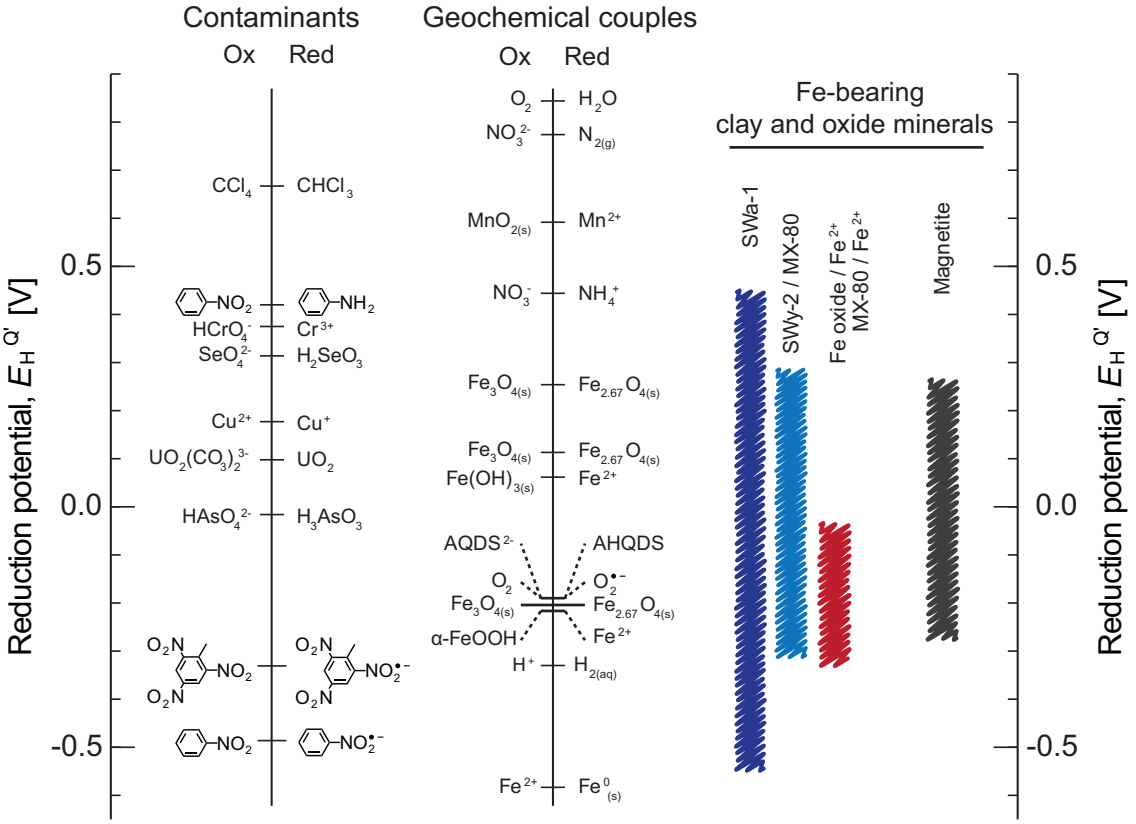

Fig. 13: Reduction potentials E_H of important organic and inorganic contaminants, geochemical redox couples, and of different Fe-bearing clay minerals and mixed phases investigated there.

Bars for Fe-bearing clay minerals and Fe^{2+}/goethite/clay mineral systems represent results from the current project. Data for magnetite from references (Gorski et al. 2010, Latta et al. 2012b).

With regard to the characterization of MX-80 bentonite, our study suggests that this material might be involved in various redox processes if used as buffer material in radioactive waste repositories. Even in its native state, MX-80 exposed to dissolved Fe^{2+} may be redox-active in the EH-range between 0 and -300 mV and control the oxidation state and thus the mobility of various radionuclides and contaminants. Our first tentative comparison of the redox properties of Fe oxides and clay minerals in mixed phase systems further shows that under repository like conditions, an identification of secondary mineral phases from steel canister corrosion will be key to assess the repositories' apparent reduction potential. We speculate that interactions of Fe^{2+} with the predominant solid Fe phase will act as redox buffer, while other that is less abundant phases act as Fe^{2+} sorbents. Determining the EH-value of such systems is possible with mediated electrochemical techniques. This option opens new avenues for the assessment of redox processes in the context of safety analyses for nuclear waste repositories.

5 References

Aeschbacher, M., Sander, M. & Schwarzenbach, R. (2010): Novel electrochemical approach to assess the redox properties of humic substances. Environ. Sci. Technol. 44/1, 87-93.

Aeschbacher, M., Vergari, D., Schwarzenbach, R.P. & Sander, M. (2011): Electrochemical analysis of proton and electron transfer equilibria of the reducible moieties in humic acids. Environ. Sci. Technol. 45/19, 8385-8394.

Aeschbacher, M., Brunner, S.H., Schwarzenbach, R.P. & Sander, M. (2012a): Assessing the effect of humic acid redox state on organic pollutant sorption by combined electrochemical reduction and sorption experiments. Environ. Sci. Technol. 46/7, 3882-3890.

Aeschbacher, M., Graf, C., Schwarzenbach, R.P. & Sander, M. (2012b): Antioxidant properties of humic substances. Environ. Sci. Technol. 46/9, 4916-4925.

Amonette, J.E. & Templeton, J.C. (1998): Improvements to the quantitative assay of non-refractory minerals for Fe(ii) and total Fe using 1,10-Phenanthroline. Clays Clay Miner. 46/1, 51-62.

Anastacio, A.S., Aouad, A., Sellin, P., Fabris, J.D., Bergaya, F. & Stucki, J.W. (2008): Characterisation of a redox-modified clay mineral with respect to its suitability as a barrier in radioactive waste confinement. Appl. Clay Sci. 39/3-4, 172-179.

Baeyens, B. & Bradbury (1997): A mechanistic description of Ni and Zn sorption on Na-montmorillonite. Part I: Titration and sorption measurements. J. Contam. Hydrol. 27/3-4, 199-222.

Bard, A.J. & Faulkner, L.R. (2001a): Electrochemical Methods: Fundamentals and Applications. John Wiley & Sons, Inc., 2nd edition.

Bard, A.J. & Faulkner, L.R. (2001b): Electrochemical Methods: Fundamentals and Applications. John Wiley & Sons, Inc., 2nd edition.

Beard, B.L., Handler, R.M., Scherer, M.M., Wu, L.L., Czaja, A.D., Heimann, A. & Johnson, C.M. (2010): Iron isotope fractionation between aqueous ferrous iron and goethite. Earth Planet. Sci. Lett. 295/1-2, 241-250.

Besson, G., Bukin, A.S., Dainyak, L.G., Rautureau, M., Tsipurskii, S.I., Tchoubar, C. & Drits, V.A. (1983): Use of diffraction and Moessbauer methods for the structural and crystallochemical characterisation of nontronites. J. Appl. Crystallogr. 16/4, 374-383.

Bradbury, M. & Baeyens, B. (2005a): Experimental measurements and modelling of sorption competition on montmorillonite. Geochim. Cosmochim. Acta 69/17, 4187-4197.

Bradbury, M. & Baeyens, B. (2005b): Modelling the sorption of Mn(II), Co(II), Ni(II), Zn(II), Cd(II), Eu(III), Am(III), Sn(IV), Th(IV), Np(V) and U(VI) on montmorillonite: Linear free energy relationships and estimates of surface binding constants for some selected heavy metals and actinides. Geochim. Cosmochim. Acta 69/4, 875-892.

Bradbury, M. & Baeyens, B. (2009a): Sorption modelling on illite. Part I: Titration measurements and the sorption of Ni, Co, Eu and Sn. Geochim. Cosmochim. Acta 73/4, 990-1003.

Bradbury, M. & Baeyens, B. (2009b): Sorption modelling on illite. Part II: Actinide sorption and linear free energy relationships. Geochim. Cosmochim. Acta 73/4, 1004-1013.

Bzdek, B.R. & McGuire, M.M. (2009): Polarized ATR-FTIR investigation of Fe reduction in the Uley nontronites. Clays Clay Miner. 57/2, 227-233.

Carlson, L., Karnland, O., Olsson, S., Rance, A. & Smart, N. (2006): Experimental studies on the interactions between anaerobically corroding iron and bentonite. Posiva Working Report 2006-06. POSIVA, Olkiluoto.

Cashion, J.D., Gates, W.P. & Thomson, A. (2008): Mössbauer and IR analysis of iron sites in four ferruginous smectites. Clay Minerals 43/1, 83-93.

Cashion, J.D., Gates, W.P. & Riley, G.M. (2010): Origin of the two quadrupole doublets in Nau-1 nontronite. J. Phys. Conf. Ser. 217, 012-065.

Castro, P., Vago, E. & Calvo, E. (1996): Surface electrochemical transformations on spinel iron oxide electrodes in aqueous solutions. J. Chem. Soc., Faraday Trans. 92/18, 3371-3379.

Charradi, K., Forano, C., Prevot, V., Amara, A.B. & Mousty, C. (2009): Direct electron transfer and enhanced electrocatalytic activity of hemoglobin at iron-rich clay modified electrodes. Langmuir 25/17, 10376-10383.

Cwiertny, D., Handler, R., Schaefer, M., Grassian, V. & Scherer, M. (2008): Interpreting nano-scale size-effects in aggregated fe-oxide suspensions: reaction of Fe(II) with goethite. Geochim. Cosmochim. Acta 72/5, 1365-1380.

Dainyak, L.G., Zviagina, B.B., Rusakov, V.S. & Drits, V.A. (2006): Interpretation of the nontronite-dehydroxylate Mössbauer spectrum using EFG [electric field gradient] calculations. Eur. J. Mineral. 18/6, 753-764.

Dong, H., Jaisi, D., Kim, J. & Zhang, G. (2009): Microbe-clay mineral interactions. American Mineralogist 94/11-12, 1505-1519.

Drits, V.A. & Manceau, A. (2000): A model for the mechanism of Fe^{3+} to Fe^{2+} reduction in dioctahedral smectites. Clays Clay Miner. 48/2, 185-195.

Dyar, M.D. (1987): A review of Mossbauer data on trioctahedral micas: Evidence for tetrahedral Fe^{3+} and cation ordering. Am. Mineral. 72/1-2, 102-112.

Dyar, M., Schaefer, M., Sklute, E. & Bishop, J. (2008): Mössbauer spectroscopy of phyllosilicates: effects of fitting models on recoil-free fractions and redox ratios. Clay Minerals 43/1, 3-33.

Fialips, C.-I., Huo, D., Yan, L., Wu, J. & Stucki, J.W. (2002a): Effect of Fe oxidation state on the IR spectra of garfield nontronite. American Mineralogist 87/5-6, 630-641.

Fialips, C.-I., Huo, D., Yan, L., Wu, J. & Stucki, J.W. (2002b): Infrared study of reduced and reduced-reoxidized ferruginous smectite. Clays Clay Miner. 50/4, 455-469.

Fultz, M. L. & Durst, R. A. (1982): Mediator compounds for the electrochemical study of biological redox systems: A compilation. Anal. Chim. Acta 140/1, 1-18.

Gailhanou, H., van Miltenburg, J.C., Rogez, J., Olives, J., Amouric, M., Gaucher, E.C. & Blanc, P. (2007): Thermodynamic properties of anhydrous smectite MX-80, illite IMt-2 and mixed-layer illite-smectite ISCz-1 as determined by calorimetric methods. Part I: Heat capacities, heat contents and entropies. Geochim. Cosmochim. Acta 71/22, 5463-5473.

Gates, W., Winkinson, H.T. & Stucki, J.W. (1993): Swelling properties of microbially reduced ferruginous smectite. Clays Clay Miner. 41/3, 360-364.

Gates, W., Stucki, J. & Kirkpatrick, R. (1996): Structural properties of reduced upton montmorillonite. Phys. Chem. Minerals 23/8, 535-541.

Gates, W.P., Jaunet, A.M., Tessier, D., Cole, M.A., Wilkinson, H.T. & Stucki, J.W. (1998): Swelling and texture of iron-bearing smectites reduced by bacteria. Clays Clay Miner. 46, 487-497.

Gates, W.P., Slade, P.G., Manceau, A. & Lanson, B. (2002): Site occupancies by iron in nontronites. Clays Clay Miner. 50/2, 223-239.

Goodman, B.A., Russell, J.D., Fraser, A.R. & Woodhams, F.W.D. (1976): A Mössbauer and I.R. spectroscopic study of the structure of nontronite. Clays Clay Miner. 24/2, 53-59.

Gorski, C.A. & Scherer, M.M. (2009): Influence of magnetite stoichiometry on Fe(II) uptake and nitrobenzene reduction. Environ. Sci. Technol. 43/10, 3675-3680.

Gorski, C.A. & Scherer, M.M. (2011): Fe^{2+} sorption at the fe oxide-water interface: A revised conceptual framework. *In:* Tratnyek, P.G., Grundl, T.J. & Haderlein, S.B. (eds.), Aquatic Redox Chemistry, volume 1071 of ACS Symposium Series, 315-343. American Chemical Society.

Gorski, C.A., Nurmi, J.T., Tratnyek, P.G., Hofstetter, T.B. & Scherer, M.M. (2010): Redox behavior of magnetite: Implications for contaminant reduction. Environ. Sci. Technol. 44/1, 55-60.

Gorski, C., Handler, R., Beard, B., Pasakarnis, T., Johnson, C. & Scherer, M. (2012a): Fe atom exchange between aqueous Fe^{2+} and magnetite. Environ. Sci. Technol. 46/22, 12399-12407.

Gorski, C.A., Aeschbacher, M., Soltermann, D., Voegelin, A., Baeyens, B., Marques-Fernandes, M., Hofstetter, T.B. & Sander, M. (2012b): Redox properties of structural Fe in clay minerals: 1. Electrochemical quantification of electron donating and accepting capacities of smectites. Environ. Sci. Technol. 46/17, 9360-9368.

Gorski, C.A., Klüpfel, L., Voegelin, A., Sander, M. & Hofstetter, T.B. (2012c): Redox properties of structural Fe in clay minerals: 2. Electrochemical and spectroscopic characterisation of electron transfer irreversibility in ferruginous smectite, SWa-1. Environ. Sci. Technol. 46/17, 9369-9377.

Gorski, C.A., Klüpfel, L., Voegelin, A., Sander, M. & Hofstetter, T.B. (2013): Redox properties of structural Fe in clay minerals: 3. Electrochemical and spectroscopic characterisation of different smectite clay minerals. Environ. Sci. Technol., *submitted*.

Grygar, T. (1997): Dissolution of pure and substituted goethites controlled by the surface reaction under conditions of abrasive stripping voltammetry. J. Solid State Electrochem. 1/1, 77-82.

Grygar, T., Marken, F., Schröder, U. & Scholz, F. (2002): Electrochemical analysis of solids. A review. Collection of Czechoslovak chemical communications 67/2, 163-208.

Harvey Jr, A., Smart, J. & Amis, E. (1955): Simultaneous spectrophotometric determination of iron(II) and total iron with 1,10-phenanthroline. Anal. Chem. 27/1, 26-29.

Hofstetter, T.B., Heijman, C.G., Haderlein, S.B., Holliger, C. & Schwarzenbach, R.P. (1999): Complete reduction of TNT and other (poly)nitroaromatic compounds under iron reducing subsurface conditions. Environ. Sci. Technol. 33/9, 1479-1487.

Hofstetter, T.B., Schwarzenbach, R.P. & Haderlein, S.B. (2003): Reactivity of Fe(II) species associated with clay minerals. Environ. Sci. Technol. 37/3, 519-528.

Hofstetter, T.B., Neumann, A. & Schwarzenbach, R.P. (2006): Reduction of nitroaromatic compounds by Fe(II) species associated with iron-rich smectites. Environ. Sci. Technol. 40/1, 235-242.

Hunter, D.B. & Bertsch, P.M. (1994): In-situ measurements of tetraphenylboron degradation kinetics on clay mineral surfaces by IR. Environ. Sci. Technol. 28/4, 686-691.

Hunter, D.M., Gates, W.P., Bertsch, P.M. & Kemner, K.M. (1999): Degradation of tetraphenylboron at hydrated smectite surfaces studied by time-resolved IR and X-ray absorpton spectroscopies. *In:* Sparks, D.L. & Grundl, T.J. (eds.), ACS Symposium Series 715, 282-300.

Hunter, F., Bate, F., Heath, T. & Hoch, A. (2007): Geochemical investigation of iron transport into bentonite as steel corrodes. SKB Technical Report TR-07-09. Swedish Nuclear Fuel and Waste Management Co., Stockholm.

Ilton, E., Heald, S., Smith, S., Elbert, D. & Liu, C. (2006): Reduction of uranyl in the interlayer region of low iron micas under anoxic and aerobic conditions. Environ. Sci. Technol. 40/16, 5003-5009.

Jaisi, D.P., Kukkadapu, R.K., Eberl, D.D. & Dong, H. (2005): Control of Fe(III) site occupancy on the rate and extent of microbial reduction of Fe(III) in nontronite. Geochim. Cosmochim. Acta 69/23, 5429-5440.

Jaisi, D.P., Dong, H., Plymale, A.E., Fredrickson, J.K., Zachara, J.M., Heald, S. & Liu, C. (2009): Reduction and long-term immobilisation of technetium be Fe(II) associated with clay mineral nontronite. Chem. Geol. 264/1-4, 127-138.

Karnland, O., Olsson, S. & Nilsson, U. (2006): Mineralogy and sealing properties of various bentonites and smectite-rich clay materials. SKB Technical Report TR-06-30. Swedish Nuclear Fuel and Waste Management Co., Stockholm.

Kim, J., Dong, H., Seabaugh, J., Newell, S. & Eberl, D. (2004): Role of microbes in the smectite-to-illite reaction. Science 303/5659, 830-832.

Klausen, J., Tröber, S., Haderlein, S.B. & Schwarzenbach, R.P. (1995): Reduction of substituted nitrobenzenes by Fe(II) in aqueous mineral suspensions. Environ. Sci. Technol. 29/9, 2396-2404.

Komadel, P., Lear, P. & Stucki, J. (1990): Reduction and reoxidation of nontronite: Extent of reduction and reaction rates. Clays Clay Miner. 38/2, 203-208.

Komadel, P., Madejova, J. & Stucki, J.W. (1995): Reduction and reoxidation of nontronite: Question of reversibility. Clays Clay Miner. 43/1, 105-110.

Komadel, P., Madejova, J. & Bujdak, J. (2005): Preparation and properties of reduced-charge smectites – A review. Clays Clay Miner. 53/4, 313-334.

Komadel, P., Madejova, J. & Stucki, J.W. (2006): Structural Fe(III) reduction in smectites. Applied Clay Science 34/1-4, 88-94.

Kostka, J., Wu, J., Nealson, K. & Stucki, J. (1999): The impact of structural Fe(III) reduction by bacteria on the surface chemistry of smectite clay minerals. Geochim. Cosmochim. Acta 63/22, 3705-3713.

Kumpulainen, S., Carlsson, T., Muurinen, A., Kiviranta, L. & Svensson, D. (2010): KBS-3H – IRON-BENTONITE INTERACTIONS: Long-term (8 – 10 y) alteration of bentonite and porewater in the presence of metallic iron. Technical Report, B+Tech and VTT.

Larese-Casanova, P. & Scherer, M.M. (2007): Fe(II) sorption on hematite: New insights based on spectroscopic measurements. Environ. Sci. Technol. 41/2, 471-477.

Latta, D.E., Bachman, J.E. & Scherer, M.M. (2012a): Fe electron transfer and atom exchange in goethite: Influence of Al-substitution and anion sorption. Environ. Sci. Technol. 46/19, 10614-10623.

Latta, D.E., Gorski, C.A., Boyanov, M.I., O'Loughlin, E.J., Kemner, K.M. & Scherer, M.M. (2012b): Influence of magnetite stoichiometry on U(VI) reduction. Environ. Sci. Technol. 46/2, 778-786.

Lear, P.R. & Stucki, J.W. (1987): Intervalence electron transfer and magnetic exchange in reduced nontronite. Clays Clay Miner. 35/5, 373-378.

Lear, P.R. & Stucki, J.W. (1989): Effects of iron oxidation state on the specific surface area of nontronite. Clays Clay Miner. 37/6, 547-552.

Lee, K., Kostka, J.E. & Stucki, J.W. (2006): Comparisons of structural Fe reduction in smectites by bacteria and dithionite: An infrared spectroscopic study. Clays Clay Miner. 54/2, 195-208.

Liger, E., Charlet, L. & Cappellen, P.V. (1999): Surface catalysis of uranium(VI) reduction by iron(II). Geochim. Cosmochim. Acta 63/19-20, 2939-2955.

Luca, V. (1991): ^{57}Fe Mössbauer spectroscopic study of structural changes during dehydration of nontronite: Effect of different exchangeable cations. Clays Clay Miner. 39/5, 478-489.

Madsen, F.T. (1998): Clay mineralogical investigations related to nuclear waste disposal. Clay Minerals 33/1, 109-129.

Manceau, A., Drits, V.A., Lanson, B., Chateigner, D., Wu, J., Huo, D., Gates, W.P. & Stucki, J.W. (2000a): Oxidation-reduction mechanism of iron in dioctahedral smectites: II. Crystal chemistry of reduced Garfield nontronite. American Mineralogist 85/1, 153-172.

Manceau, A., Lanson, B., Drits, V. A., Chateigner, D., Gates, W.P., Wu, J., Huo, D. & Stucki, J.W. (2000b): Oxidation-reduction mechanism of iron in dioctahedral smectities: I. Crystal chemistry of oxidized reference nontronites. American Mineralogist 85/1, 133-152.

Meckstroth, M.L., Norris, B.J. & Heineman, W.R. (1981): 387 – mediator-titrants for thinlayer spectroelectrochemical measurement of biocomponent u◦' and n values. Bioelectroch. Bioener. 8/1, 63-70.

Mikutta, C., Wiederhold, J.G., Cirpka, O.A., Hofstetter, T.B., Bourdon, B. & von Gunten, U. (2009): Iron isotope fractionation and atom exchange during sorption of ferrous Fe to mineral surfaces. Geochim. Cosmochim. Acta 73/7, 1795-1812.

Milodowski, A., Cave, M., Kemp, S., Taylor, B., Green, K., Williams, C. & Shaw, R. (2009a): Mineralogical investigations of the interaction between iron corrosion products and bentonite from the NF-Pro experiments (phase 1). SKB Technical Report TR-09-02. Swedish Nuclear Fuel and Waste Management Co., Stockhom.

Milodowski, A., Cave, M., Kemp, S., Taylor, B., Green, K., Williams, C. & Shaw, R. (2009b): Mineralogical investigations of the interaction between iron corrosion products and bentonite from the NF-Pro experiments (phase 2). SKB Technical Report TR-09-03. Swedish Nuclear Fuel and Waste Management Co., Stockholm.

Nagra (2002a): Project Opalinus Clay – Models, Codes and Data for Safety Assessment: Demonstration of disposal feasibility for spent fuel, vitrified high-level waste and long-lived intermediate-level waste (Entsorgungsnachweis). Nagra Technical Report NTB 02-06. Nagra, Wettingen.

Nagra (2002b): Project Opalinus Clay – Safety Report: Demonstration of disposal feasibility for spent fuel, vitrified high-level waste and long-lived intermediate-level waste (Entsorgungsnachweis). Nagra Technical Report NTB 02-05. Nagra, Wettingen.

Neumann, A., Hofstetter, T.B., Lussi, M., Cirpka, O.A. & Schwarzenbach, R.P. (2008): Assessing the redox reactivity of structural iron in smectites using nitroaromatic compounds as kinetic probes. Environ. Sci. Technol. 42/22, 8381-8387.

Neumann, A., Hofstetter, T.B., Skarpeli-Liati, M. & Schwarzenbach, R.P. (2009): Reduction of polychlorinated ethanes and carbon tetrachloride by structural Fe(II) in smectites. Environ. Sci. Technol. 43, 4082-4089.

Neumann, A., Petit, S. & Hofstetter, T.B. (2011a): Evaluation of redox-active iron sites in smectites using middle and near infrared spectroscopy. Geochim. Cosmochim. Acta 75/9, 2336-2355.

Neumann, A., Sander, M. & Hofstetter, T.B. (2011b): Redox properties of structural Fe in smectite clay minerals. *In:* Tratnyek, P.G., Grundl, T.J. & Haderlein, S.B. (eds.), Aquatic Redox Chemistry, volume 1071 of ACS Symposium Series, 361-379. American Chemical Society.

Neumann, A., Olson, T.L. & Scherer, M.M. (2013): Spectroscopic evidence for Fe(II)-Fe(III) electron transfer at clay mineral edge and basal sites. Environ. Sci. Technol. 47/13, 6969-6977.

Nurmi, J.T. & Tratnyek, P.G. (2008): Electrochemical studies of packed iron powder elecrodes: Effects of common constituents of natural waters on corrosion potential. Corrosion Sci. 50/1, 144-154.

Nurmi, J.T., Bandstra, J.Z. & Tratnyek, P.G. (2004): Packed powder electrodes for characterizing the reactivity of granular iron in borate solutions. J. Electrochem. Soc. 151/6, B347-B353.

Page, S.E., Sander, M., Arnold, W.A. & McNeill, K. (2012): Hydroxyl radical formation upon oxidation of reduced humic acids by oxygen in the dark. Environ. Sci. Technol. 46/3, 1590-1597.

Pecher, K., Haderlein, S.B. & Schwarzenbach, R.P. (2002): Reductive of polyhalogenated methanes by surface-bound Fe(II) in aqueous suspensions of iron oxides. Environ. Sci. Technol. 36/8, 1734-1741.

Rancourt, D.G. & Ping, J.Y. (1991): Voigt-based methods for arbitrary-shape static hyperfine parameter distributions in Mössbauer spectroscopy. Nuclear Instruments and Methods in Physics Research, Section B: Beam Interactions with Materials and Atoms 58/1, 85-97.

Ravel, B. & Newville, M. (2005): ATHENA, ARTEMIS, HEPHAESTUS: data analysis for X-ray absorption spectroscopy using IFEFFIT. J. Synchrotron Rad. 12/4, 537-541.

Ribeiro, F.R., Fabris, J.D., Kostka, J.E., Komadel, P. & Stucki, J.W. (2009): Comparisons of structural iron reduction in smectites by bacteria and dithionite: II. A variable-temperature Mossbauer spectroscopic study of Garfield nontronite. Pure Appl. Chem. 81/8, 1499-1509.

Rozenson, I. & Heller-Kallai, L. (1976): Reduction and oxidation of Fe^{3+} in dioctahedral smectites: 1: Reduction with hydrazine and dithionite. Clays Clay Miner. 24, 271-282.

Russell, J.D., Goodman, B.A. & Fraser, A.R. (1979): Infrared and Mössbauer studies of reduced nontronites. Clays Clay Miner. 27/1, 63-71.

Schaefer, M.V., Gorski, C.A. & Scherer, M.M. (2011): Spectroscopic evidence for interfacial Fe(II)-Fe(III) electron transfer in a clay mineral. Environ. Sci. Technol. 45/2, 540-545.

Silvester, E., Charlet, L., Tournassat, C., Gehin, A., Greneche, J.-M. & Liger, E. (2005): Redox potential measurements and Mossbauer spectrometry of Fe(II) adsorbed onto Fe(III) (oxyhydr)oxides. Geochim. Cosmochim. Acta 69/20, 4801-4815.

Soltermann, D., Fernandes Marques, M., Baeyens, B., Dähn, R., Miehé-Brendlé, J., Wehrli, B. & Bradbury, M.H. (2013): Fe(II) sorption on a synthetic montmorillonite. A combined macroscopic and spectroscopic study. Environ. Sci. Technol. 47/13. 6978-6986.

Stucki, J.W. (1981): The quantitative assay of minerals for Fe^{2+} and Fe^{2+} ions using 1,10-phenanthroline: II. A photochemical method. Soil Sci. Soc. Am. J. 45/3, 638-641.

Stucki, J.W., Golden, D.C. & Roth, C.B. (1984): Preparation and handling of dithionite-reduced smectite suspensions. Clays Clay Miner. 32/3, 191-197.

Stucki, J.W., Bailey, G.W. & Gan, H. (1996): Oxidation-reduction mechanisms in iron-bearing phyllosilicates. Applied Clay Science 10/6, 417-430.

Stucki, J.W., Wu, J., Gan, H.M., Komadel, P. & Banin, A. (2000): Effects of iron oxidation state and organic cations on dioctahedral smectite hydration. Clays Clay Miner. 48/2, 290-298.

Stucki, J.W., Lee, K., Zhang, L. & Larson, R.A. (2002): Effects of iron oxidation state on the surface and structural properties of smectites. Pure Appl. Chem. 74/11, 2145-2158.

Stumm, W. & Morgan, J.J. (1996): Aquatic Chemistry. Wiley Intersciences, 3rd edition.

Stumm, W. & Sulzberger, B. (1992): The cycling of iron in natural environments: Considerations based on laboratory studies of heterogeneous redox processes. Geochim. Cosmochim. Acta 56, 3233-3257.

Therias, S., Mousty, C., Forano, C. & Besse, J.P. (1996): Electrochemical transfer at anionic clay modified electrodes. Case of 2,2'-azinobis(3-ethylbenzothiazoline-6-sulfonate). Langmuir 12/20, 4914-4920.

Vantelon, D., Montarges-Pelletier, E., Michot, L.J., Briois, V., Pelletier, M. & Thomas, F. (2003): Iron distribution in the octahedral sheet of dioctahedral smectites. An FeK-edge X-ray absorption spectroscopy study. Phys. Chem. Minerals 30/1, 44-53.

Wilke, M., Farges, F., Petit, P., Brown, G. & Martin, F. (2001): Oxidation state and coordination of Fe in minerals: An Fe K-XANES spectroscopic study. American Mineralogist 86/5-6, 714-730.

Williams, A.G.B. & Scherer, M.M. (2004): Spectroscopic evidence for Fe(II)-Fe(III) electron transfer at the iron oxide-water interface. Environ. Sci. Technol. 38/18, 4782-4790.

Xiang, Y. & Villemure, G. (1995): Electrodes modified with synthetic clay-minerals – evidence of direct electron-transfer from structural iron sites in the clay lattice. J. Electroanal. Chem. 381/1-2, 21-27.

Yan, L. & Stucki, J.W. (2000): Structural perturbations in the solid-water interface of redox transformed nontronite. J. Colloid Interface Sci. 225/2, 429-439.

Yanina, S.V. & Rosso, K.M. (2008): Linked reactivity at mineral-water interfaces through bulk crystal conduction. Science 320/5873, 218-222.